USE OF ADAPTIVE FILTERING TECHNIQUES FOR ESTIMATING

LOW-FREQUENCY ELECTROMECHANICAL MODES IN POWER SYSTEMS

By

Ashok Balasubramanian

RECOMMENDED:

Advisory Committee Chair

Chair, Department of Electrical and Computer Engineering

APPROVED:

Dean, College of Engineering and Mines

Dean of the Graduate School

June 19, 2006

Date

USE OF ADAPTIVE FILTERING TECHNIQUES FOR ESTIMATING LOW-FREQUENCY ELECTROMECHANICAL MODES IN POWER SYSTEMS

A

THESIS

Presented to the Faculty

of the University of Alaska Fairbanks

in Partial Fulfillment of the Requirements

for the Degree of

MASTER OF SCIENCE

By

Ashok Balasubramanian, B.E.

Fairbanks, Alaska

August 2006

Abstract

Information about the location and strength of low frequency electromechanical modes in power systems reflects the stability of the system. Highly recommended and used techniques like Prony analysis and eigenanalysis require ring down from a disturbance and tedious matrix calculations, respectively, for mode estimation. This work proposes the use of the Least Mean Squares (LMS) adaptive filtering algorithms and its combination with other algorithms for estimating and tracking the modes with respect to time. The mode of interest in this work was the 0.26 Hz mode. An Adaptive Step Size Least Mean Squares (ASLMS) algorithm was introduced in this work to reduce variability in mode estimation for non-stationary environments. The ASLMS algorithms achieved quicker convergence than LMS algorithms. A combination of the ASLMS and the LMS algorithm called the Error Tracking (ET) algorithm was tested, based on the running error in the estimate, to reduce variability while also maintaining reasonable convergence time. The ET algorithm achieved high accuracy, less variable performance and quicker convergence of estimates compared to all the other algorithms. The ET algorithm tracked the 0.26 Hz mode in both the simulated data and the real time data with the least amount of error.

Table of Contents

Page
Signature Page i
Title Page ii
Abstract iii
Table of Contents iv
List of Figures vii
List of Tables xiv
Acknowledgements xv

Chapter 1 Introduction 1

(1.1) Power System Stability 3
(1.2) Electromechanical Modes 7
(1.3) Measurement Based Data Analysis 9
(1.4) Contributions of this Work 11

Chapter 2 Evaluation and Processing of Simulated and Ambient Power System Data 13

(2.1) 19-Machine Simulated Data 13
(2.2) Real Time (Ambient) Power System Data 18
2.2.1 Pre-Processing of Simulated and Ambient Power System Data 20
(2.3) Determination of Location (Frequency) of Modes in the Megawatt Signals 21

Chapter 3 Adaptive Filtering Techniques for Mode Estimation 27

(3.1) History and Classes of Adaptive Filters 27
(3.2) Least Mean Squares (LMS) Algorithm 28
3.2.1 Structure and Operation of LMS Algorithm 29

3.2.2 Convergence of LMS Algorithm 31
(3.3) The Misadjustment Parameter 32
(3.4) Combining LMS and AR Algorithms.....33
3.4.1 LMS Mode Tracking with Initial AR Estimates 34
3.4.2 LMS Mode Tracking with Previous LMS Estimates.....38

Chapter 4 Adaptive Step Size Least Mean Squares (ASLMS) Algorithm 39

(4.1) Constraints of Adaptive Algorithm in Non-stationary Environments.....39
(4.2) LMS Algorithm in Non-stationary Environments 41
(4.3) Degree of Non-stationarity 43
(4.4) Modified LMS Algorithm for Performance in Non-stationary Environments.....45

Chapter 5 Application of LMS Algorithm, Combination Algorithms and ASLMS Algorithm on Test System Data 49

(5.1) LMS Result with a Cold Start 49
5.1.1 LMS Results with Previous Estimates from AR Block-processing 51
(5.2) Results from ASLMS Algorithm 54
(5.3) Error Tracking (ET) Algorithm 61

Chapter 6 Application of LMS Algorithm, Combination Algorithms and ASLMS Algorithm on Ambient Power System Data.....65

(6.1) Estimating Electromechanical Modes in June 7, 2000, MR #1 Ambient Data.....66
6.1.1 Dominant Mode Identification using Auto-Regressive Block-processing...67
6.1.2 LMS Result with a Cold Start 68
6.1.3 LMS Results with Previous Estimates from AR Block-processing 69

6.1.4 Results from ASLSM Algorithm 73
(6.2) Estimating Electromechanical Modes in June 13, 2000, MR #1 Ambient Data.....78
6.2.1 Results from AR Block-processing 79
6.2.2 LMS Results with Cold Start 80
6.2.3 LMS Results with Previous Estimates from AR Block-processing 81
6.2.4 Results from ASLSM Algorithm 85
(6.3) Performance of Error Tracking Algorithm 90

Chapter 7 Conclusions and Future Work 93

(7.1) Conclusions 93
(7.2) Future Work 96

List of Figures

		Page
Figure 1.1:	Power signal from Malin-Round Mountain #1 showing breakup of August 10, 1996 (Time reference: 15:35:30 PM PST) [1].....	4
Figure 1.2:	Growing oscillations from Malin-Round Mountain #1 during August 10, 1996 event (Time reference: 15:36:30 PM PST) [1].....	5
Figure 1.3:	Mechanical analogy of an interconnected power system.....	6
Figure 1.4:	Pole with characteristic frequency and damping ratio representing an electromechanical mode.....	8
Figure 2.1:	19-machine simulated system	14
Figure 2.2:	One minute real-power flow on line 17 from bus 22 to bus 26 of the 19-machine system	15
Figure 2.3:	Power Spectral Density of the real-power flow for line 17 from bus 22 to bus 26 measured over a time period of one hour.....	16
Figure 2.4:	General map of the Western North America power system [1].....	19
Figure 2.5:	Two minutes of megawatt data from June 7, 2000 using the Malin-Round Mountain #1 signal. Note: Time Reference: 14:28:05 PM PST.....	20
Figure 2.6:	Two minutes of pre-processed megawatt data from June 7, 2000 using the Malin-Round Mountain #1 signal Note: Time Reference: 14:28:05 PM PST	21
Figure 2.7:	Power Spectral Density of the real-power flow on June 7, 2000 using MR #1 signal.	23
Figure 2.8:	Power Spectral Density of the real-power flow on June 13, 2005 using MR #1 signal	23
Figure 2.9:	Spectrogram of line 17 for one hour of simulated data from the 19-machine system	24

Figure 2.10: Spectrogram of 18 minutes of ambient data on June 7, 2000 from MR #1. Note: Time Reference: 14:28:05 PM PST..... 25

Figure 2.11: Spectrogram of 48 hours ambient data on June 13, 2005 from MR #1. Note: Time Reference: 06:00:05 AM 25

Figure 3.1: Prediction class of adaptive algorithm 28

Figure 3.2: Schematic representing LMS filtering algorithms 29

Figure 3.3: AR block-processing model with white noise as input 35

Figure 4.1: Line dynamic model of a non-stationary environment [17] 42

Figure 4.2: Multi regression model incorporated in an adaptive filter for use in non-stationary environments 44

Figure 4.3: Block diagram of ASLMS algorithm [17] 47

Figure 5.1: Mode frequency vs. time for the megawatt data between buses 22 and 26 of the 19-machine system. (60 minutes, cold start and μ = 7.8231 e-04, 3.5560 e-04 and 1.4224 e-04)..... 50

Figure 5.2: Damping ratio vs. time for the megawatt data between buses 22 and 26 of the 19-machine system. (60 minutes, cold start and μ = 7.8231 e-04, 3.5566 e-04 and 1.4224 e-04)..... 51

Figure 5.3: Mode frequency vs. time for the megawatt data from the 19-machine system between buses 22 and 26 of the 19-machine system. (60 minutes, μ = 3.556 e-05, weight vector from AR for different block sizes)..... 52

Figure 5.4: Damping ratio vs. time for the megawatt data of the 19-machine system between buses 22 and 26 of the 19-machine system. (60 minutes and μ = 3.556 e-05, weight vector from AR for different block sizes)..... 53

Figure 5.5: Mode frequency vs. time by cold start for the megawatt data of the 19-machine system between buses 22 and 26 of the 19-machine system, initial estimate from 10 minutes run into previous LMS run and initial weight vector from AR block processing..... 54

Figure 5.6: Damping ratio vs. time using cold start for the megawatt data of the 19-machine system between buses 22 and 26 of the 19-machine system, initial estimate from 10 minutes into previous LMS run and initial weight vector from AR block processing..... 55

Figure 5.7: Mode frequency vs. time for megawatt data of the 19-machine system between buses 22 and 26 of the 19-machine system (60 minutes, cold start, LMS: μ=7.8231 e-06, ASLMS: μ=7.8231 e-06, ρ = 1.8182 e-03)..... 56

Figure 5.8: Damping ratio vs. time for megawatt data of the 19-machine system between buses 22 and 26 of the 19-machine system (60 minutes, cold start, LMS: μ=7.8231 e-06, ASLMS: μ=7.8231 e-06, ρ = 1.00 e-03)..... 57

Figure 5.9: Mode frequency vs. time for the 19-machine megawatt data between buses 22 and 26 of the 19-machine system (60 minutes, cold start, μ=7.8231 e-06, ρ=1.82 e-03, 1.00 e-03, 5.55 e-04)..... 58

Figure 5.10: Damping ratio vs. time for the 19-machine megawatt data between buses 22 and 26 of the 19-machine system (60 minutes, cold start, μ=7.8231 e-06, ρ=2.50 e-03, 1.43 e-03, 2.85 e-04)..... 59

Figure 5.11: Mode frequency vs. time for megawatt data of the 19-machine system between buses 22 and 26 (60 minutes, μ=7.8231 e-07, LMS-ASLMS: ρ=2.00 e-03, ASLMS-LMS: ρ=5.71 e-03) 60

Figure 5.12: Damping ratio vs. time for megawatt data of the 19-machine system between buses 22 and 26 (60 minutes, μ=7.8231 e-07, LMS-ASLMS: ρ=2.00 e-03, ASLMS-LMS: ρ=5.00 e-03)..... 61

Figure 5.13: Mode frequency vs. time for megawatt data between buses 22 and 26 of the 19-machine system (60 minutes, cold ASLMS start ASLMS: μ=7.8231 e-07, ρ=0.04 and LMS: μ=7.8231 e-08)..... 63

Figure 5.14: Damping ratio vs. time for megawatt data between buses 22 and 26 of the 19-machine system (60 minutes, cold ASLMS start ASLMS: μ=7.8231 e-07, ρ=0.02 and LMS: μ=7.8231 e-08)..... 63

Figure 6.1: One-minute of preprocessed megawatt data from Malin-Round Mountain #1 on June 7, 2000 (Time Reference: 14:28:05 PM PST)... 66

Figure 6.2: Mode frequency vs. time of MR #1, June 7, 2000 data (cold start: μ = 2.1862 e-05, 8.7448 e-06 and 3.9352 e-06)..... 68

Figure 6.3: Mode damping ratio vs. time of MR #1, June 7, 2000 data (cold start: μ= 2.1862 e-05, 8.7448 e-06 and 3.9352 e-06)..... 69

Figure 6.4: Mode frequency vs. time of MR #1, June 7, 2000 data (18.84 minutes, μ = 8.7448 e-07, weight vector from AR for different block sizes)..... 70

Figure 6.5: Mode damping ratio vs. time of MR #1, June 7, 2000 data (18.84 minutes, μ = 8.7448 e-07, weight vector from AR for different block sizes)..... 71

Figure 6.6: Mode frequency vs. time using cold start, using an initial weight vector from 10 minutes into the previous run, and using an initial weight vector from AR block processing with a 10 minute block size of MR #1, June 7, 2000 data..... 72

Figure 6.7: Mode damping ratio vs. time using cold start, using an initial weight vector from 10 minutes into the previous run, and using an initial weight vector from AR block processing with a 10 minute block size of MR #1, June 7, 2000 data..... 72

Figure 6.8: Mode frequency vs. time for MR #1, June 7, 2000 data. (18.85 minutes, cold start, LMS: μ=8.7448 e-07, ASLMS: μ=8.7448 e-07, ρ = 6.67 e-06)..... 74

Figure 6.9: Damping ratio vs. time for MR #1, June 7, 2000 data (18.85 minutes, cold start, LMS: μ=8.7448 e-07, ASLMS: μ=8.7448 e-07, ρ = 2.00 e-06)..... 74

Figure 6.10: Mode frequency vs. time for MR #1, June 7, 2000 data (18.85 minutes, cold start, μ=8.7448 e-07 and ρ=1.00 e-05, 6.67 e-06, 4.00 e-06)..... 75

Figure 6.11: Damping ratio vs. time for MR #1, June 7, 2000 data (18.85 minutes, cold start, μ=8.7448 e-07 and ρ=5.00 e-06, 2.00 e-06, 1.42 e-06)..... 76

Figure 6.12: Mode frequency vs. time for MR #1, June 7, 2000 data (18.85 minutes, μ=8.7448 e-08, LMS-ASLMS: ρ=1.33 e-06 ASLMS-LMS: ρ=6.67 e-06)..... 77

Figure 6.13: Damping ratio vs. time for MR #1, June 7, 2000 data (18.85 minutes, μ=8.7448 e-08, LMS-ASLMS: ρ=8.33 e-06, ASLMS-LMS: ρ=1.42 e-05)..... 77

Figure 6.14: One-minute of preprocessed megawatt data from Malin-Round Mountain #1 on June 13, 2005. (Time Reference: 06:00:15 AM PST)..... 78

Figure 6.15: Mode frequency vs. time for MR #1 June 13, 2005 data (180 minutes, cold start: μ = 3.3715 e-06, 1.5418 e-06 and 6.2537 e-07)..... 80

Figure 6.16: Mode damping ratio vs. time for MR #1 June 13, 2005 data (180 minutes) (cold start: μ = 3.3715 e-06, 1.5418 e-06 and 6.2537e-07)... 81

Figure 6.17: Mode frequency vs. time for MR #1 June 13, 2005 data (180 minutes, μ = 1.5418 e-07, weight vector from AR for different block sizes)..... 82

Figure 6.18: Mode damping ratio vs. time for MR #1 June 13, 2005 data (180 minutes, μ = 1.5418e-07, weight vector from AR for different block sizes)..... 82

Figure 6.19: Mode frequency vs. time for the MR #1 June 13, 2005 data, using cold start, using an initial weight vector from 10 minutes into the previous run, and using an initial weight vector from AR block processing with a 10 minute block size..... 83

Figure 6.20: Mode damping ratio vs. time for the MR #1 June 13, 2005 ambient data using cold start, using an initial weight vector from 10 minutes into the previous run, and using an initial weight vector from AR block processing with a 10 minute block size..... 84

Figure 6.21: Mode frequency vs. time for MR #1 June 13, 2005 data (18.85 minutes, cold start, LMS: μ=3.3715 e-06, ASLMS: μ=3.3715 e-06, ρ = 5.43 e-10)..... 86

Figure 6.22: Damping ratio vs. time for MR #1 June 13, 2005 data (180 minutes, cold start, LMS: μ=3.3715 e-06, ASLMS: μ=3.3715 e-06, ρ = 6.94 e-10)..... 86

Figure 6.23: Mode frequency vs. time for MR #1 June 13, 2005 data (180 minutes, cold start, μ=3.3715 e-06 and ρ=6.94 e-10, 5.43 e-10 and 2.50 e-10) 87

Figure 6.24: Damping ratio vs. time for MR #1 June 13, 2005 data (180 minutes, cold start, μ=3.3715 e-06 and ρ=6.94 e-10, 5.31 e-10 and 2.38 e -10)..... 88

Figure 6.25: Mode frequency vs. time for MR #1 June 13, 2005 data (180 minutes, μ=3.3715 e-07, LMS-ASLMS: ρ=1.53 e-07 ASLMS-LMS: ρ=2.5 e-08)..... 89

Figure 6.26: Damping ratio vs. time for MR #1 June 13, 2005 data (180 minutes, μ=3.3715 e-07, LMS-ASLMS: ρ=1.12 e-07, ASLMS-LMS: ρ=4.08 e-08)..... 89

Figure 6.27: Mode frequency vs. time for MR #1 June 7, 2000 data (18.85 minutes, cold ASLMS start ASLMS: μ=8.7448 e-07, ρ=6.25 e-05 and LMS: μ=8.7448 e-08)..... 91

Figure 6.28: Damping ratio vs. time for MR #1 June 7, 2000 data (18.85 minutes, cold ASLMS start ASLMS: μ=8.7448 e-07, ρ=1.00 e-05 and LMS: μ=8.7448 e-08)..... 91

Figure 6.29: Mode frequency vs. time for MR #1 June 13, 2005 data (180 minutes, cold ASLMS start ASLMS: μ=3.3715 e-07, ρ=4.08 e-08 and LMS: μ=3.3715 e-08)..... 92

Figure 6.30: Damping ratio vs. time for MR #1 June 13, 2000 data (180 minutes, cold ASLMS start ASLMS: μ=3.3715 e-07, ρ=4.25 e-08 and LMS: μ=3.3715 e-08)..... 92

List of Tables

Page

Table 1.1: Mechanical equivalents of electrical power systems 6

Table 2.1: Frequency and damping ratio for stationary 19-machine modes 17

Table 2.2: Frequency and damping ratios for stationary 19-machine case 18

Table 6.1: Degree of non-stationarity of ambient data sets 65

Table 6.2: Frequency and percent damping ratio estimates using AR block-processing of MR #1-2000 data 67

Table 6.3: Frequency and percent damping ratio estimates using AR block-processing of MR #1 2005 data..... 79

Acknowledgements

The author would like to acknowledge the following people for their contribution and support in this work:

Dr. Richard Wies, for serving as my advisor during my time here at the University of Alaska Fairbanks. Your constant enthusiasm, support, patience and most of all your belief in me made every task easier and enjoyable.

Dr. Vikas Sonwalkar and Dr. Seta Bogosyan, for serving on my advisory committee and always being available to help.

Dr. J. W. Piere, for his useful hints and comments which were helpful in publishing my results and work in conference proceedings for the conferences to be held in June, 2006, and in journal publications, for which manuscripts are under preparation.

I would like to thank the Bonneville Power Administration for funding this work under Grant 00012512. I would also like to thank the U.S. Department of Energy and EPSCoR for funding this work under grant DE-FC02-91ER75680.

I thank my friends Ashish, Arun, Sri, Tomas Marsik, Bala and Tipsi for their constant support and encouraging words during times of distress.

Finally, I would like to expresses my sincerest gratitude to my father and mother.

Chapter 1
Introduction

The stability of large interconnected power systems is a primary goal in transmitting power without any major disturbances. Every generator connected in these large systems should operate in synchrony to achieve stability. The sudden loss of electrical output power from a generator or group of generators operating in parallel forces other generators in the system to pick up the load. This sudden transfer of load between two generators due to the sudden failure of one is called swinging. Swinging causes large oscillations in the flow of power in the transmission line as all generators are interconnected. Since these oscillations tend to originate from the imbalance of mechanical input power and electrical output power of the generator they are referred to as electromechanical oscillations or electromechanical modes.

Estimation of low frequency electromechanical modes is important for assessing the stability of interconnected power systems. The two basic approaches for mode estimation are model based and measurement based. Model based approaches depend on building a physical model similar to the system under study. The model should possess all the characteristics of the original power system. Since the original power system is too large and has complex interconnections, building a simplified model with all the characteristics of the original system is not possible. Also building of such a model demands extensive computations. Measurement based approaches described as follows estimate the low frequency electromechanical modes from measured real-time power system data. Eigenanalysis requires the calculation of eigenvalues of the system under study and involves tedious computations [1]. Spectral analysis, an extension of FFT analysis, however, gives information only about the frequency (location) of the electromechanical modes [1]. No information about the rate of damping of the electromechanical mode is available from spectral analysis. Prony analysis has been the most extensively used and a credible measurement based technique [1]. Prony analysis requires a ring down from a disturbance for estimating the modes in the data. More

information about spectral analysis, eigenanalysis and Prony analysis are mentioned in section three of Chapter One (1.3). Block processing and adaptive filtering techniques have been explored as mode estimation techniques [1]. These techniques do not require a ring down from a disturbance for estimating the modes. Block processing techniques are point based algorithms. They return the frequency and damping of the electromechanical mode based on the block size of data considered and return a single value of the mode at the end of the block size. Adaptive filtering techniques are algorithms which continuously estimate and track frequency and damping of electromechanical modes over time. Thus by using adaptive filtering techniques the modes can be tracked close to real-time.

The goal of the work performed in this thesis is to explore different combinations of block processing and adaptive filtering techniques in estimating the electromechanical modes. An adaptive filtering algorithm is also studied for performance in non-stationary environments. These adaptive filtering algorithms and the combination of techniques aim to achieve the following:

- Reduced error in frequency and damping ratio estimates.
- Less variability between two iterations in estimating the frequency and damping ratio of the electromechanical modes.
- Reduced convergence time of algorithms in tracking frequency and damping ratio of electromechanical modes.

The long term goal of this research is to design an adaptive filtering algorithm or design a combination of block processing and adaptive filtering algorithms which will continuously monitor the electromechanical modes in power systems. The designed algorithm should be able to monitor the modes accurately with small windows of data. This algorithm could be incorporated in a mode meter with a green/yellow/red indicator which indicates the position and the strength of a particular mode. The mode meter would be a valuable measurement tool for determining stability of power systems.

1.1 Power System Stability

Stability is the ability of a power system to remain in synchronous equilibrium under steady state operating conditions and to regain a state of equilibrium after a disturbance occurs [2]. Synchronous equilibrium is reached in a power system when all the generators connected to the system operate at the same frequency. Large disturbances can be due to severe lightning strikes, bad weather conditions like ice storms causing huge system faults and major equipment losses [2]. The most frequent disturbances occur in the form of rapid load changes. All generators connected to the system operate at a constant frequency of 60 Hz. In meeting the demands of a rapid load change, the balance between the mechanical input power and the electrical output power is lost. The system frequency falls when the load increases and rises when the load decreases. This is because as the load increases suddenly the speed of the synchronous generators connected to this system tends to slow down. The frequencies of operation of the generators also drop from their previous value to match to this new speed. Due to the changes in demand some generators may speed up and some generators may slow down and thus the synchronism between all the generators is lost. Large oscillations tend to originate in the real power due to these imbalances. Usually when a system moves towards instability, the frequency of the mode drops due to the rapid changes in load. An electromechanical mode exhibiting a sudden drop in mode frequency and damping ratio implies the possibility of a growing oscillation and hence instability.

Power outages are direct consequences of large oscillations. The black out in August 1996 is a classic example. Figure 1.1 [1] shows the flow of 1400 MW from Oregon to California at Malin-Round Mountain #1 in the western US grid. The figure shows the final events in the power system before the oscillations that caused the black out. The frequency of the 0.28 Hz mode drops from 0.276 Hz to 0.252 Hz due to a sudden drop in load caused by the trip of the Keeler–Allston line. The damping ratio drops from as high as 7.0 % to 1.2 %. The damping ratio goes negative when the oscillations start growing and the system become negatively damped and unstable. Figure

1.2 shows the growing oscillations that caused this impending outage. There was no flow of power on the line after the growing oscillations, when the circuit breakers tripped the line out of service. This case gives us a classical understanding of why electromechanical modes should be monitored close to real time and how possible black-outs can be avoided in doing so.

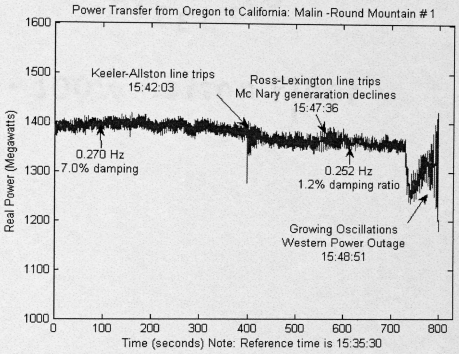

Figure 1.1: Power signal from Malin-Round Mountain #1 showing breakup of August 10, 1996 (Time reference: 15:35:30 PM PST) [1].

The mechanical analogy of an interconnected power system can be illustrated with balls of different sizes connected to each other by strings [3]. The mechanical analogy is shown in Figure 1.3 with a list of equivalent terms in Table 1.1. The balls 1-8 represent the generators. The strings represent the transmission lines. All the balls are connected to each other through strings. The thick strings are connected to each other by thinner strings representing smaller interconnections in power systems.

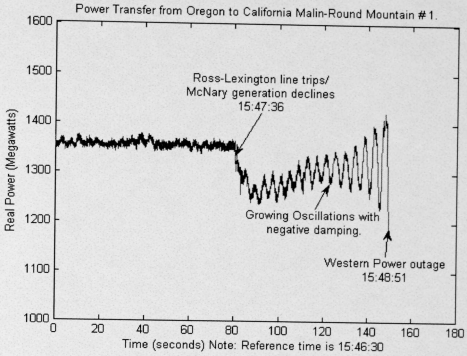

Figure 1.2: Growing oscillations from Malin-Round Mountain # 1 during August 10, 1996 event (Time reference: 15:36:30 PM PST) [1].

Now if ball 7 is made to swing by striking it, the two strings connected to ball 7 and the strings connected to these strings and hence balls 1, 3 and 8 start swinging. The balls connected to balls 1, 3 and 8 through other strings also oscillate. Thus the whole mechanical system starts oscillating. If these oscillations continue to grow then a string may break and cause instability in the whole system. The other possible occurrence would be damped oscillations and the entire system returning to steady state. The loaded capacity of the system plays an important role in defining the stability of the system. A disturbance in a heavily loaded system can cause instability, while the system may come back to equilibrium after a disturbance of some magnitude if it is lightly loaded. This condition can be explained by a suitable analogy using a pitcher and a marble [3].

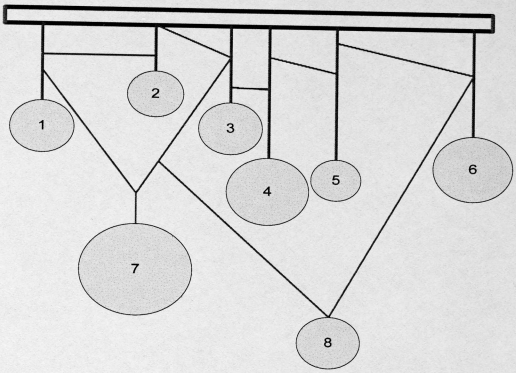

Figure 1.3: Mechanical analogy of an interconnected power system.

Table 1.1: Mechanical equivalents of electrical power systems

Electrical machines and terms	Mechanical equivalent
Generator	Balls
Transmission Lines	Strings
Equilibrium	Rest
Electrical oscillations	Swings
Stability	Rest

If a pitcher representing the power system is half filled with water and is subjected to a disturbance by dropping a marble, the water will not splash out indicating stability of the system. Similarly, the pitcher filled to its rim representing a power system operating closer to its stability limits, and if subjected to the same disturbance, will splash the water over the rim of the pitcher indicating instability.

1.2 Electromechanical Modes

A disturbance in a power system causes a group of generators to go out of step. This demands other group of generators to adapt quickly to a new state of operation causing large oscillations in the system. A lot of information can be gathered about the stability of the system from the nature of these oscillations. Whenever a disturbance occurs there is a frequency swing between two groups of generators for the reasons mentioned in Section 1.1. These frequency swings are normally between 0.1 to 3.0 Hz and are commonly referred to as electromechanical modes. The electromechanical modes are classified according to their relative frequency locations as [4, 5]:

1. Inter-area modes occur when machines in one part (area) of the system swing against machines in another part (area) of the system. The characteristic frequencies of inter-area modes of oscillation range from 0.1 to 0.6 Hz.
2. Local modes occur when machines in the same area, whether with in the same plant or between different plants, swing against each other with a characteristic frequency of 0.8 to 2 Hz.
3. Intra-plant modes occur when machines in the same power plant swing against each other with a characteristic frequency ranging from 1.5 to 3.0 Hz.

These modes are also direct consequences of random load changes. The stability of the power system can be assessed by the frequency and strength of the low frequency electromechanical modes in the system. One example of a heavily loaded transmission line prone to random load changes is the power line from British Columbia to California. The power line carries 2300 MW of power from Canada into the United States. Under peak load conditions due to very high demand from summer air conditioning loads this line operates closer to stability limits. The grid this line connects to exhibits electromechanical mode frequencies near 0.26 Hz, 0.45 Hz and 0.6 Hz [6].

While analyzing the stability of a power system the frequency and the damping ratio of the electromechanical modes should be considered. Frequency measurements give the actual location of the electromechanical modes and damping ratio measurements define the strength of the system. Damping ratio is a measure of opposition given by the system to the oscillatory behavior. The higher the damping ratio the less chance of oscillations in the power system. Figure 1.4 shows a pole with characteristic frequency (ω_d) and damping ratio (ξ) representing an electromechanical mode.

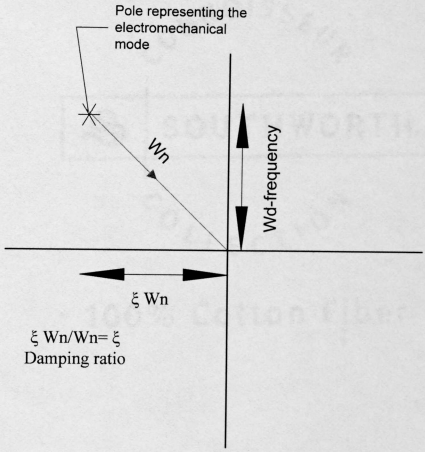

Figure 1.4: Pole with characteristic frequency and damping ratio representing an electromechanical mode.

Assuming a stationary frequency ω_d, the farther the pole is to the left of the $j\omega$ axis, the higher the damping ratio and the higher the stability of the system. When a system starts oscillating it is understood that the damping ratio decreases and the pole moves closer to the $j\omega$ axis. When a pole crosses to the right of the $j\omega$ axis, instability

occurs and the system starts to exhibit growing oscillations. This type of system is referred to as a negatively damped system.

1.3 Measurement Based Data Analysis

The advantages of measurement based data analysis are two fold:

- It does not require development of accurate models of the power system under study.
- It is capable of continuously monitoring the modes in the system and also keeps track of changes in mode frequency and damping ratio.

These techniques only require monitoring and recording power system ambient (real-time) data. Events such as swings and oscillations due to random load changes and disturbances are also recorded in the power system data. The randomness of these swings shows up as noise in the actual data. The primary component of noise is most likely due to random load changes [7, 8]. Assuming that the noise is white over the frequency range of interest, signal processing techniques can be used to estimate the low frequency electromechanical modes in power systems. This assumption was verified by calculating the power spectral density of the power system signal. The results of the power spectral density for the power system data are shown in Chapter 2.

There are several measurement based techniques available for estimating the modes in power system data. Eigenanalysis is one of the earliest methods used for the purposes of mode estimation. Unlike previous methods which relied on fitting a linear model of the power system and then determining the eigenvalues of the linear system, eigenanalysis linearizes the nonlinear power system to identify the eigenvalues [9]. A plant matrix is constructed which contains information about the frequency of the modes in the form of the square root of eigenvalues calculated [10]. The plant matrix is given by [10]

$$\mathbf{A} = \begin{bmatrix} 0 & \mathbf{I} \\ [\mathbf{M}]^{-1}[\mathbf{K}] & 0 \end{bmatrix} \qquad \text{(Eq 1.1)}$$

where [M] is a diagonal matrix containing information about the inertia constants of the generator and the matrix [K] contains information about the output power and the rotor angle of the generator. However, the plant matrix is built by neglecting the flux decay, damper and governor effects [11] and considering the power output and rotor angle of the generator only. The solution becomes complex if the flux decay, dampers and the excitation are considered in the design. Thus this method demands a lot of computation. Advances in the eigenvalue solution approach and the use of high frequency computer processors have helped to achieve the complex eigensolution more easily.

The Fast Fourier Transform (FFT) method involves analysis of noise signals to compute the spectral content of the signal. The FFT of a signal $x(k)$ is given by

$$X(n) = \sum_{k=0}^{N-1} x(k)\, e^{-j\omega_0 k\Delta t} \quad \text{, where } \omega = 2*\text{pi}*\, n*\Delta\, f\,. \qquad \text{(Eq 1.2)}$$

FFT analysis provides information about the oscillating frequencies and their respective magnitudes. No information about the damping ratio of the mode is available from the spectral analysis. The relative oscillations of one part of the system with respect to an other part of the system are determined by comparing the phase sequence of the common mode frequencies.

Prony analysis [12, 13] is one of the most credible techniques used in this field. Prony analysis is an extension of FFT analysis that estimates both the frequency and the damping ratio of electromechanical modes. Since Prony analysis does not identify the system transfer function, it requires a ring down from a disturbance to analyze the mode frequency and damping ratio. To achieve a good estimation from Prony analysis without a ringdown, signals with large amplitudes need to be injected into the power system to get reasonable signal to noise ratio. However, this may generate large disturbances in the

power system. Injection of Low-Level Pseudo-Random Noise (LLPRN) with small amplitude and long duration works as a good substitute for break insertions (large resistor banks) under normal operating conditions since the injection of LLPRN does not cause large disturbances in the power system [14]. The Numerical Algorithm for Subspace State Space System Identification (N4SID) applied to the LLPRN test data can be used to estimate electromechanical modes. However, N4SID requires tedious Henkel matrix calculations and the state space model demands multiple outputs of a system model for accuracy [14].

The adaptive filtering and block processing techniques like those used in this work help in continuously monitoring both the frequency and damping ratio and require no ring down from a disturbance. These algorithms use ambient power system data to estimate the mode frequency and damping ratio. The variability and time of convergence of the estimates from these algorithms are the most important factors to be considered for which different combinations of adaptive filtering and block processing techniques are developed in this work. An adaptive filtering algorithm with an adaptive step size parameter is also developed as a part of this work with the assumption that the power system data are non-stationary.

1.4 Contributions of this Work

The objective of this work was to develop an adaptive filtering algorithm that would estimate and track the electromechanical modes in the power system data with:

- Reduced error in its frequency and damping ratio estimates.
- Less variability between two iterations in estimating the frequency and damping ratio of the electromechanical modes.
- Reduced convergence time of algorithms in tracking frequency and damping ratio of electromechanical modes.

The following contributions were made in this work to felicitate the tracking performance and achieve the above objectives:

- Using an initial weight vector from AR block processing algorithm in the LMS algorithm to reduce the variability and time of convergence of the LMS algorithm tracking performance.
- Introducing an Adaptive Step-Size Least Mean Squares (ASLMS) algorithm to promote faster convergence performance in tracking.
- Executing different combinations of the LMS and ASLMS algorithms to reduce the variability in ASLMS estimates.
- Introducing an Error Tracking (ET) algorithm to estimate and track the electromechanical mode with higher accuracy, less variability and less time of convergence.

Chapter 2

Evaluation and Processing of Simulated and Ambient Power System Data

The power system data used for this work consisted of two types: simulated power system data and actual ambient power system data. The simulated data was generated from a 19-machine test system and the ambient data was collected from the Dittmer monitor located in the Northwest US power grid. The advantage of using the 19-machine simulated system was the knowledge of the location and behavior of the modes in the data. This information was used to compare with results from the adaptive filtering techniques. Once these techniques proved credible they could be applied to actual power system megawatt data for mode estimation.

2.1 19-Machine Simulated Data

Power system models such as the 19-machine system discussed in this section are actually developed to monitor the behavior of a respective power system under different circumstances and operating conditions. The 19-machine system shown in Figure 2.1 is a reduced order model of the western North American power system originally constructed by the authors of [15] and later developed in MATLAB® by Dr. Dan Trudnowski at Montana Tech. The simulated system was used to generate power system data with inherent random load variations. Power System Toolbox [16] in MATLAB® was used to write the code for the construction of the test system. The random load variations that are added to the power system data at a given sampling rate show up in the megawatt data of the simulated system as noise, thus generating noisy megawatt data similar to actual power system data. The simulated data consist of both stationary and moving modes.

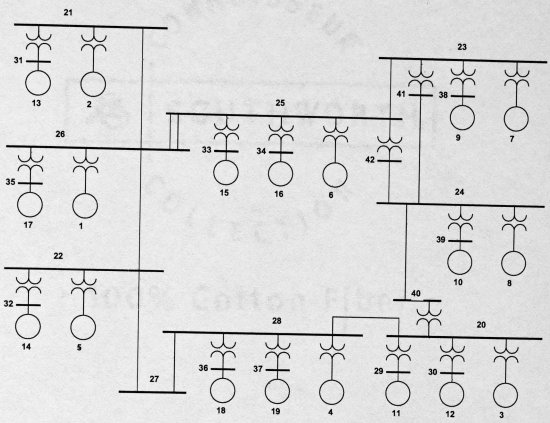

Figure 2.1: 19-machine simulated system.

The 19-machine system consisted of five inter-area modes and several local modes. Generators 1 through 8 were modeled with relatively larger inertias compared to other generators in order to provide the desired inter-area mode frequencies and shapes. Except for generator 15, all the generators used in building the simulated system were modeled as classical machines. Generator 15 was modeled as a detailed sub-transient machine with an exciter. Generators 9 through 19 were modeled to run with inputs from steam turbines on their governors. The loads in the system were modeled as constant power loads and as constant current loads, representing real power loads and reactive power loads, respectively. The resulting non-linear power system with all the generators and loads tied together was linearized, using the Power System Tool Box [16], into a linear system of 92^{nd} order. The load modulations at the real power and reactive power loads on buses 20 through 28 were modeled as independent Gaussian random load modulations and adjusted so that 1% of the total load was represented as random. The real power flow from bus 22 to bus 26 is shown in Figure 2.2 with the mean value removed from the data. The mean value was removed from the data as a requirement for

an input to the LMS adaptive filter. LMS is a zero mean process. The type of convergence of the LMS filter used for this work as explained in Chapter 3 is convergence in mean square. For such a type of convergence the mean value of the tap inputs have to be zero for a low value of mean square error. Thus having a zero mean process as input to the LMS filter will reduce the variability of LMS estimates. The real power data in the figure shows the random nature of the power system megawatt data.

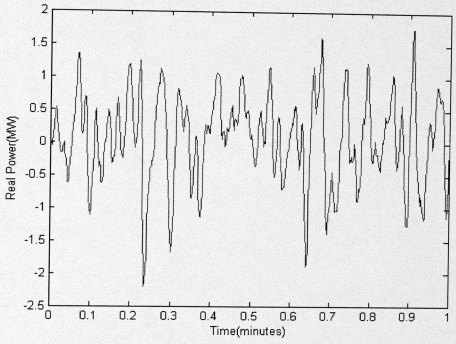

Figure 2.2: One minute real-power flow on line 17 from bus 22 to bus 26 of the 19-machine system.

The Power Spectral Density of the real-power flow from bus 22 to bus 26 was estimated using the psd function in MATLAB®. Input parameters used for the psd function were the following: input data, 512 sample hamming window with a 50% overlap (256 samples), a 1024 sample FFT window and a sampling frequency of 5 Hz. The power spectral density of the simulated power system data is shown in Figure 2.3. Figure 2.3 shows an inter area mode at 0.26 Hz. The peaks near 1.7 Hz are local modes.

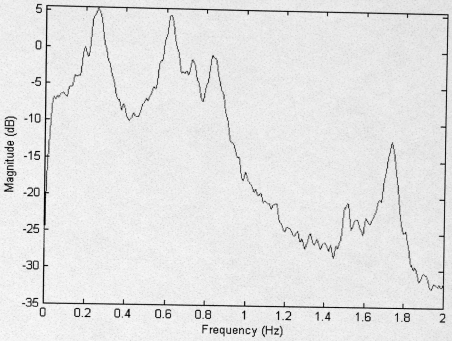

Figure 2.3: Power Spectral Density of the real-power flow for line 17 from bus 22 to bus 26 measured over a time period of one hour.

Three different types of simulations were carried out with the 19-machine system. The simulations are: (a) purely stationary, (b) stationary with a fault and (c) exponential variation (ramping). The purely stationary modes were generated at 10 samples per second. The location (frequency) and strength (damping ratio) of the stationary modes are shown in Table 2.1. The stationary mode with a fault consists of two separate modes, a pre-fault mode and a post-fault mode. When using the pre-fault mode the mode frequency measured at 0.32 Hz is dropped to 0.26 Hz after the fault, while the damping ratio of the mode moves from 4.99% before the fault to 0.65% after the fault. The frequency and damping ratio of the stationary modes with the fault case are shown in Table 2.2. The ramping case involves a moving mode. The movement of the mode may be either exponential or linear. The mode frequency gradually decreases from 0.32 Hz.

Table 2.1: Frequency and damping ratio for stationary 19-machine modes

Frequency (Hz)	Damping Ratio (%)
0.2624	10.33
0.5835	3.93
0.6202	3.86
0.7347	3.17
0.8432	2.81

The data generated with a stationary mode were processed before mode estimation to improve mode identification efficiency and accuracy. Initial steps of pre-processing involved subtraction of the mean value from the data for purposes mentioned earlier in this section (page 15) and decimation of the sampling frequency from 10 samples/second to 5 samples/second. The reasons for decimation are two fold [8]. The first purpose of decimation is to satisfy the Nyquist criterion. Inter-area modes and local modes range from 0.1 to 0.6 Hz and 0.8 to 2 Hz, respectively. So, in order to look at modes below 2.5 Hz, the sampling frequency of the system was set at a frequency greater than or equal to a frequency twice the highest frequency in the system (2.5 Hz). The second reason for decimation is to reduce the filter order. Filter orders are always proportional to the sampling frequency. By keeping the sampling frequency low, the filter order and the number of filter coefficients are also kept low.

Table 2.2: Frequency and damping ratios for stationary 19-machine case with a fault

Pre-Fault		Post-Fault	
Frequency (Hz)	Damping Ratio (%)	Frequency (Hz)	Damping Ratio (%)
0.0459	39.1630	0.0458	36.5957
0.3244	4.9923	0.2568	6.9490
0.5995	2.0322	0.5478	2.1160
0.6753	2.1600	0.6643	2.1125
0.7890	1.6283	0.7472	1.6613

2.2 Real Time (Ambient) Power System Data

The ambient power system data were collected from the western North American power grid. Two separate sets of ambient data were used for this work. The two power flows were recorded from the same monitors: the real-power flow from Malin-Round Mountain #1 (MR #1) at the California-Oregon inter-tie on June 7, 2000 for 18.85 minutes and the real power flow on June 13, 2005 for 48 hours. The data do not contain a ring down from a break insertion or a fault that can be analyzed with a Prony fit. Figure 2.3 shows a general map of the western North American power grid provided by John Hauer at PNNL [1].

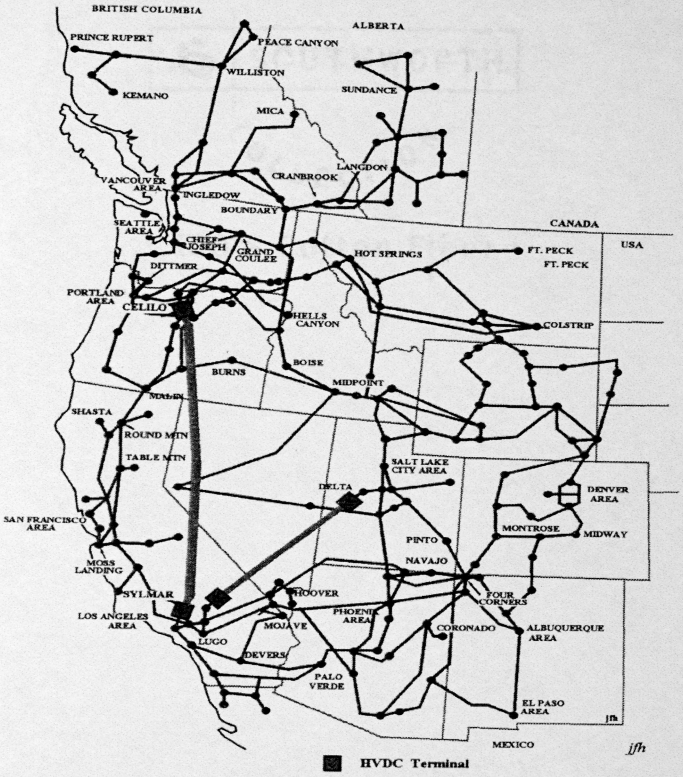

Figure 2.4: General map of the Western North America power system [1].

2.2.1 Pre-processing of Simulated and Ambient Power System Data

The underlying assumptions in dealing with power system data in mode identification and estimation are the same for both simulated power system data and the ambient power system data. Random load changes cause oscillations in the system which show up in the actual data as noise. Assuming that this noise is white over the frequency range of interest, adaptive filtering techniques can be applied to estimate the location and strength of the electromechanical modes. Figure 2.5 shows two minutes of megawatt data recorded from June 7, 2000, using the Malin-Round Mountain #1 signal without pre-processing. Pre-processing of ambient power system data involves three stages: low pass filtering, decimation and high pass filtering.

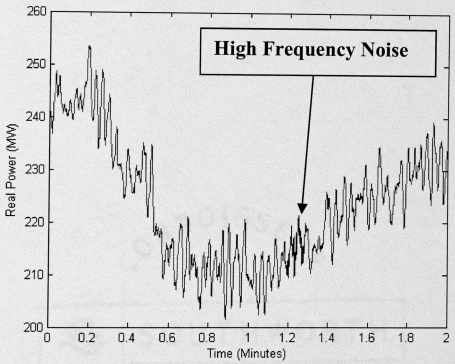

Figure 2.5: Two minutes of megawatt data from June 7, 2000 using the Malin Round Mountain #1 signal. Note: Time Reference: 14:28:05 PM PST.

After the mean value was removed from the data for purposes mentioned earlier in Section 2.1, a Parks/McClellan FIR low pass filter with a cutoff frequency of 2 Hz was used to remove the high frequency measurement noise from the data. The data was then

decimated from 10 samples/second to 5 samples/second for reasons mentioned earlier. In the third stage of the filtering process the decimated data were filtered using a high pass filter to remove very low frequency noise below 0.1Hz and any DC components. Figure 2.6 shows two minutes of processed megawatt data from June 7, 2000 using the MR #1 signal.

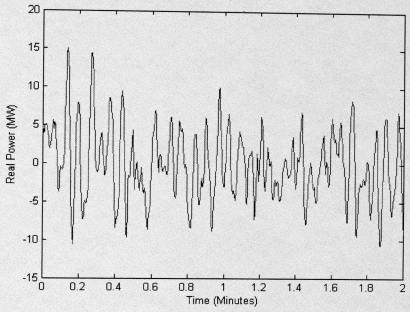

Figure 2.6: Two minutes of pre-processed megawatt data from June 7, 2000 using the Malin Round Mountain #1 signal. Note: Time Reference: 14:28:05 PM PST.

Comparing the pre-processed and un-processed data from Figure 2.5 and Figure 2.6, the real power oscillations in Figure 2.6 are around 0 MW as opposed to 230 MW in Figure 2.5 because of the removal of the mean value from the data for reasons discussed earlier in this chapter. The high frequency noise prevalent in the un-processed data (Figure 2.5) is reduced in the pre-processed data (Figure 2.6).

2.3 Determination of the Location (Frequency) of Modes in the Megawatt Signals

Unlike the simulated 19-machine megawatt data, no information regarding the frequencies of the modes was available with the ambient power system data. The Power Spectral Density (PSD) of the megawatt data proved to be useful in determining the

strength of the electromechanical modes at their respective frequencies. The PSD of the 60 minute data window of the simulated system shown in Figure 2.3 shows that the strength in the 0.26 Hz and 0.7 Hz modes is greater than the strength in the 1.5 Hz and 1.7 Hz modes. The PSD is calculated by the psd function in MATLAB®. The input parameters for the PSD function are the input data, a Hamming window with size not to be greater than the FFT window size, the FFT size, the sampling frequency and an overlap size not greater than the window size. Figure 2.7 shows the PSD of June 7, 2000 using the MR #1 signal with an FFT size of 512 points, a Hamming window size of 256, 50 % overlap and a sampling frequency of 5 Hz. Figure 2.8 shows the PSD of June 13, 2005 using the MR #1 signal with an FFT size of 1024 points, a Hamming window size of 1024 points and 50 % overlap (512 points) and a sampling frequency of 5 Hz. From Figures 2.7 and 2.8 it is observed that the inter-area modes with frequency around 0.26 Hz have the highest strength in the signal compared to other local modes. The 0.26 Hz mode is the characteristic dominant mode frequency of the western North American Power grid.

Spectrograms are a good visual for determining the frequency and relative strength of the electromechanical modes. A spectrogram computes the FFT of the overlapping blocks and displays an estimated power spectrum as a function of time. The spectrogram is plotted using the specgram function in MATLAB®. The inputs to the specgram function are the input data, the FFT size, the sampling frequency, the window size and the overlap size. The window size should have a length smaller than or equal to the FFT size and greater than the overlap size.

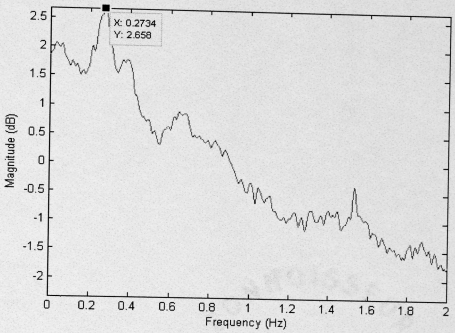

Figure 2.7: Power Spectral Density of the real-power flow on June 7, 2000 using MR #1 signal.

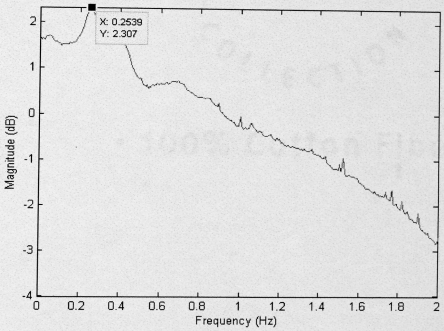

Figure 2.8: Power Spectral Density of the real-power flow on June 13, 2005 using MR #1 signal.

Figure 2.9 shows the spectrogram of the 19-machine simulated data with an FFT size of 1024 points, a Hamming window of size 512 points with a 50 % overlap and a sampling frequency of 5 Hz. The 0.26 Hz and the 0.6 Hz interarea modes can be seen and a weaker local mode can be deciphered near 1.7 Hz. Figure 2.10 and Figure 2.11 show

the spectrogram of the ambient data from June 7, 2000 and June 13, 2005, respectively.

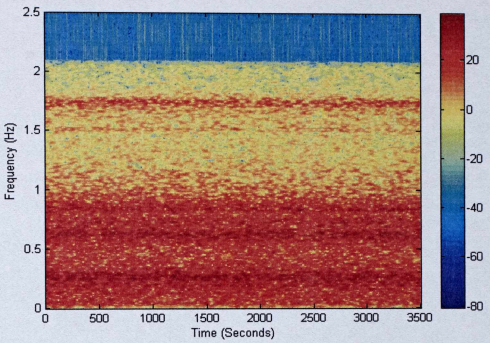

Figure 2.9: Spectrogram of line 17 for one hour of simulated data from the 19-machine system.

Figure 2.11 shows the spectrogram of the 48 hour ambient data measured from June 13, 2005 to June 15, 2005 from Malin Round Mountain #1. Comparing Figures 2.10 and 2.11 it can be seen that the oscillations in the system are lower in the June 13, 2005 data. This can be seen from the color of the 0.26 Hz inter-area mode in the spectrograms. The intensity of the color representing the 0.26 Hz mode in Figure 2.11 is less compared to the intensity of the color representing the 0.26 Hz mode in Figure 2.10. The advantage of using the power spectral density and the spectrogram on the power system megawatt data is that these techniques give an idea about the strength of both the inter-area modes and the local modes in the signal in the frequency range of interest.

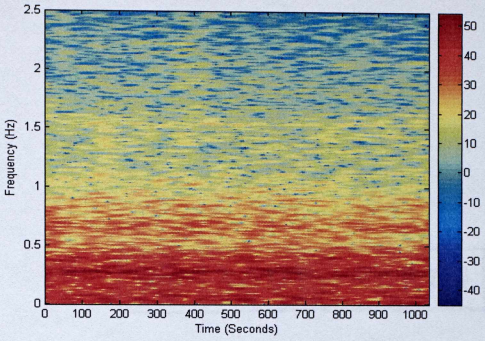

Figure 2.10: Spectrogram of 18 minutes of ambient data on June 7, 2000 from MR #1. Note: Time Reference: 14:28:05 PM PST.

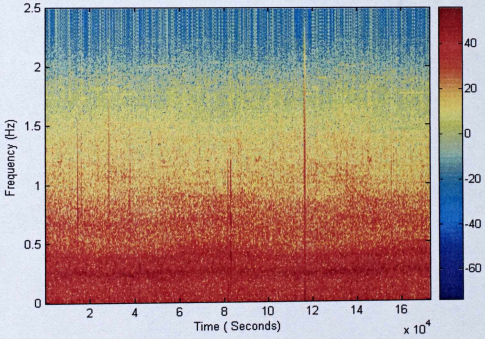

Figure 2.11: Spectrogram of 48 hours ambient data on June 13, 2005 from MR #1. Note: Time Reference: 06:00:15 AM PST.

From the PSD plots and the spectrogram plots of the power system megawatt data, the dominant mode frequency is found to be near 0.26 Hz. The dominant inter-area modes in the western North American power grid have a characteristic electromechanical

mode at 0.26 Hz. Effective adaptive filtering techniques and the combination of adaptive techniques and block-processing techniques are discussed in Chapter 3 and Chapter 4, respectively, to estimate and track the 0.26 Hz mode over the entire length of the data.

Chapter 3

Adaptive Filtering Techniques for Mode Estimation

Adaptive filters can function in an unknown environment and track the time-varying statistics in the input signal effectively. The random load variations show up in the actual power system data as noise, which is white over the frequency range of interest. Assuming that the noise is statistically stationary in the frequency range of interest, adaptive filtering techniques can be applied to power system megawatt data in order to track the electromechanical modes.

3.1 History and Classes of Adaptive Filters

All adaptive filters, irrespective of the application for which they are used, have the following features in common:

- Input vector - u
- Desired Response - d
- Estimation error - e
- Output of the adaptive filter -y.

The building blocks of the adaptive filters take different forms such as tap weight, reflection co-efficient, and rotation parameters. The essential difference among various applications of adaptive filtering lies in the way in which the desired response is extracted. Based on the extraction technique of the desired response (d), adaptive filtering techniques are classified as identification algorithms, inverse modeling algorithms, prediction algorithms, or interference cancellation algorithms [17]. The adaptive filter used in this thesis works on the principle of prediction algorithms where the present

values of the signal serve as a desired response and the past values serve as system input. Figure 3.1 shows the prediction class of adaptive filtering applications.

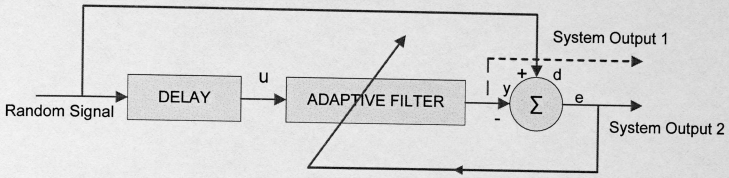

Figure 3.1: Prediction class of adaptive algorithm [17].

The history of adaptive filtering techniques takes us way back to 1632, when the theory of estimation was invented by Galileo Galilei and was used to minimize various functions of errors. Gauss, at the age of 18, in 1795, invented the method of least squares to study the motion of planetary bodies. Much work in this field was also carried out by Kalman, Hopf, and Weiner in the 1800s [17].

3.2 Least Mean Squares (LMS) Algorithm

In 1959, Windrow and Hoff invented the Least Mean Squares (LMS) algorithm during their study of pattern-recognition and defined it as a stochastic gradient algorithm that iterates each tap weight in the direction of the gradient of the squared magnitude of the error signal [17]. The most significant feature of the LMS algorithm is its simplicity.

The LMS filter consists of two basic stages:

- Filtering stage
- Adaptive stage.

In the filtering stage, the LMS filter computes the output for the given input (power system data in this case) and generates an estimation error by comparing the produced output with the desired response. The adaptive process involves automatic adjustment of filter parameters (tap weight vectors) in order to reduce the estimation error until the filter operation becomes optimized in the mean square error sense [17]. Figure 3.2 shows the schematic of the LMS filter, combining both the filtering and the adaptive process. The FIR filter is in the main loop and the adaptive weight control mechanism is formed by the feedback loop.

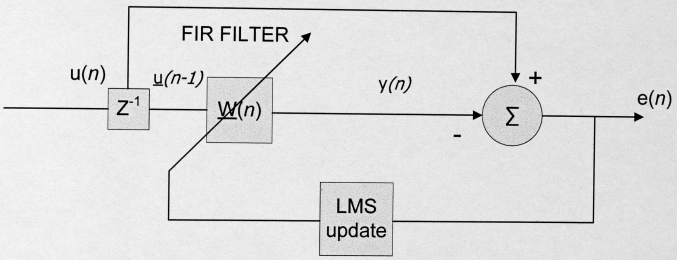

Figure 3.2: Schematic representing LMS filtering algorithms [17].

3.2.1 Structure and Operation of LMS Algorithm

The LMS filter as discussed in the previous section is a combination of a linear FIR transversal filter and an adaptive weight control mechanism. The LMS structure shown in Figure 3.2 is defined by the following three relationships [17]:

$$y(n) = \underline{w}^{H}(n)\underline{u}(n) \qquad \text{(Eq 3.1)}$$

$$e(n) = u(n) - y(n) \qquad \text{(Eq 3.2)}$$

$$\underline{w}(n+1) = \underline{w}(n) + \mu \underline{u}(n-1)e^{*}(n) \qquad \text{(Eq 3.3)}$$

where $u(n)$ is the actual power system data in the form of tap input vectors, $\underline{\mathbf{u}}(n\text{-}1) = [u(n\text{-}1)\ u(n\text{-}2). \ . \ .u(n\text{-}M)]^T$ is the data vector with M past values, $\underline{\mathbf{w}}(n) = [w_1(n)\ w_2(n)\ldots. w_M(n)]^T$ is a time-varying vector of filter tap weights, $y(n)$ is the filter output, $e(n)$ is the error output, μ is the step size parameter, and M is the filter order. As the number of iterations reaches infinity the value of the tap weight vector of the LMS filter may come close to $\underline{\mathbf{w}}_0$ (Wiener Solution) , which shows that the filter's solution is close to the optimal solution [17]. The tap weight vectors $\underline{\mathbf{w}}(n)$ generated from the LMS process can be used to track the modes of the input data $u(n)$. The modes are first tracked by finding the roots of the z-domain polynomial and are then converted to the s-plane. The z-domain polynomial is defined by

$$a(z,n) = 1 - \mathbf{w}_1(n)z^{-1} - \ldots \mathbf{w}_M(n)z^{-M}. \qquad \text{(Eq 3.4)}$$

The function used to convert the roots from the z domain to the s-domain is as follows:

$$s(n) = \ln(roots(a(z,n))) / T \qquad \text{(Eq 3.5)}$$

where T is the sampling period. The total number of roots will be equal to the filter tap length M. The information about the frequency and damping ratio of the dominant mode can be extracted from the roots and the results can be tracked over a finite length of data or over the full data length.

3.2.2 Convergence of LMS Algorithm

The LMS function allows two possible approaches for convergence. The first is convergence in the mean. The second is convergence in the mean square. Convergence in the mean square is used in this application. For wide-sense stationary data with a small μ, the LMS algorithm will converge if the step size parameter μ is set, according to the interval [17]:

$$0 < \mu < (2 / totalMSV). \qquad \text{(Eq 3.6)}$$

The total mean square value (*MSV*) equals M (number of filter weights) times the mean square value of the input data [17]

$$totalMSV = \frac{M}{L}\sum_{n=0}^{L-1} u^2(n) \qquad \text{(Eq 3.7)}$$

where u(*n*) is the noisy input data and L is the length of the noisy input data. The feedback loop acting around the FIR filter is a low-pass filter whose average time constant Γ_{avg} is inversely proportional to the step-size parameter. The adaptive processes for small step size parameters (larger time constants) are slower than those for large step-size parameters. However, the effects of gradient noise during the tap weight updates are largely filtered out. Similarly, the adaptive process is quick for larger step size parameters (smaller time constants) but the gradient noise during tap weight updates are less filtered when smaller step-size parameters are used.

The frequency and damping ratio tracking of the 19-machine simulated data are discussed in Chapter 5, and for the real ambient power system data in Chapter 6.

3.3 The Misadjustment Parameter

Since the LMS filter involves a feedback loop in its operation, stability becomes an important issue. The condition for the operation of an adaptive algorithm that is sufficiently stable is [17]:

$$J(n) \to J(\infty) \quad as \quad n \to \infty \qquad \text{(Eq 3.8)}$$

where $J(n)$ is the mean square error produced by the adaptive filter at the time n and $J(\infty)$ is the final value of mean square error. The mean square error $J(n)$ tends to the final value of mean square error $J(\infty)$ as the time n approaches infinity. The difference between the final value of mean square error $J(\infty)$ and the minimum value of mean square error $J_{\min}$ at the Wiener solution is called the excess mean square error $J_{ex}(\infty)$. The excess mean square error represents the cost borne in using the adaptive mechanism in the form of the LMS algorithm. The ratio of $J_{ex}(\infty)$ to $J_{\min}$ is called the misadjustment parameter [17] :

$$\mathcal{M} = \frac{J_{ex}(\infty)}{J_{\min}}. \qquad \text{(Eq 3.9)}$$

The misadjustment is a dimensionless parameter which gives a measure of how close the LMS algorithm result is to the optimum results. It is usually represented as a percentage. A misadjustment of 5% means that the LMS algorithm produces a mean square error that is 5% greater than the minimum mean square error $J_{\min}$. Misadjustments up to 10 % in the LMS algorithm are usually considered satisfactory for performance. Some important observations about the misadjustment parameter are listed as follows [17]:

- The misadjustment parameter ($\mathcal{M}$) is directly proportional to the step size parameter and the filter tap length M.
- The misadjustment parameter ($\mathcal{M}$) is inversely proportional to the time constant Γ_{avg} of the LMS filter.

3.4 Combining LMS and AR Algorithms

The step size parameter and the accuracy of the initial weight vector estimates determine the convergence time and variability of the frequency and damping ratio estimates. A larger step size decreases the convergence time, but increases the variability of the estimates due to the increase in estimation error described in Eq 3.3. In contrast, a smaller step size provides less variability in the estimates, but takes more time to converge. The selection of the step size parameter is the most important factor to be established for the LMS estimates to converge to the actual mode with less variability and convergence time [17]. Starting with a zero weight vector (cold start) the LMS algorithm has to update its weight vector during every iteration all the way from 0 to a value closer to a weight vector corresponding to the Wiener solution $\underline{\mathbf{w}}_0$. Under such conditions the LMS algorithm takes more time to converge and the ability to track the mode with less variability is reduced. The convergence time and the accuracy of the frequency and damping ratio estimates could be improved by starting the LMS algorithm with an initial tap weight vector closer to a tap weight vector corresponding to the Wiener solution [1, 17, and 18]. Selection of an initial tap weight vector closer to the actual value can be achieved by either one of the following methods:

- Using an initial weight vector from the Auto-Regressive (AR) block-processing algorithm.
- Using an initial weight vector from a previous LMS algorithm run on the same set of data for a shorter period of time.

3.4.1 LMS Mode Tracking with Initial AR Estimates

Among the many block-processing techniques that could be employed for mode estimation, the sliding block-processing technique was chosen for this work. The data are analyzed by sliding a window through the data in steps. The estimates are constantly updated at the end of each window length [19]. Several methods are available to implement the sliding block-processing technique among which are the Auto-Regressive (AR), Auto-Regressive Moving Average (ARMA) and Fast Fourier Transform (FFT) methods. AR and ARMA are parametric approaches while the FFT is a non-parametric approach [20]. AR and ARMA allow for the direct estimation of the modes. The AR block-processing technique was preferred in this work over the ARMA block-processing technique. The nature of AR block-processing technique being an all-pole filter excited by white noise matches the structure of the adaptive LMS algorithm. The over-determined AR approach used typically works best for cases where poles are close to the unit circle as in a power system case [20]. The technique assumes that the input is approximately white over the frequency range of interest. An AR model is described by the following differential equation [17]:

$$u(n) + a_1 u(n-1) + \cdots + a_N u(n-N) = v(n) \qquad \text{(Eq 3.10)}$$

where $a_1, \cdots, a_N$ are the coefficients that represent the poles of the system and $v(n)$ is white noise. With the white noise $v(n)$ acting as the input, we may use Eq 3.10 to produce an AR process $u(n)$ as the output. Such a filter represents a process generator. The AR process generator is an all-pole filter. Its transfer function is completely defined by the location of poles (N) and there are no zeros in the system (M=0). Figure 3.3 shows an AR model with white noise acting as the input.

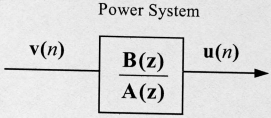

Figure 3.3: AR block-processing model with white noise as input [20].

The poles of the system are calculated by using the roots $a_1,\cdots,a_N$ of the characteristic equation $0=1+a_1(n)z^{-1}+\cdots+a_N(n)z^{-N}$. The parameters $a_1,\cdots,a_N$ are determined by deriving the covariance structure from estimates obtained from blocks of data. A relationship between the coefficients and the autocorrelation function, $r(k)=E\{u(n)\,u(n-k)\}$, of the stochastic data $u(n)$ can be derived. The difference equation Eq 3.10 can be manipulated to reveal the covariance structure.

Multiplying both sides of the difference equation Eq 3.10 by $u(n-k)$ and then taking the expected value of both sides gives [21- 22]

$$r(k)+\sum_{i=1}^{N} a_i r(k-i)=\sum_{j=0}^{M} b_j\, E\{v(n-j)\,u(n-k)\}. \qquad \text{(Eq 3.11)}$$

The right side of Eq 3.11 is equal to zero for k>*M*, as there is no correlation between the output and future input noise, so the expression reduces to [21]

$$r(k)+\sum_{i=1}^{N} a_i\, r(k-i)=0, \quad \text{for } k>M. \qquad \text{(Eq 3.12)}$$

Eq 3.12 may be rewritten as [17]:

$$r(k) = -\sum_{i=1}^{N} a_i \, r(k-i), \quad \text{for } k > M . \tag{Eq 3.13}$$

The set of equations above for $k = M+1, M+2, \cdots, M+P$ (P = the number of equations) may be expressed in matrix form using the property $r(k) = r(-k)$ [17],

$$-\underline{r} = R\underline{a} \tag{Eq 3.14}$$

where

$$\underline{r} = \begin{bmatrix} r(M+1) & r(M+2) & \cdots & r(M+P) \end{bmatrix}^T \tag{Eq 3.15}$$

and

$$R = \begin{bmatrix} r(M) & r(M-1) & \cdots & r(M-N+1) \\ r(M+1) & r(M) & \cdots & \\ \vdots & & & \vdots \\ r(M+P-1) & \cdots & & r(M-N+P) \end{bmatrix} \tag{Eq 3.16}$$

and

$$\underline{a} = \begin{bmatrix} a_1 & a_2 \cdots a_N \end{bmatrix}^T . \tag{Eq 3.17}$$

Eq 3.14 explicitly relates the auto correlation function of the input power system data to the unknown coefficients. In practice, since the true autocorrelation function values are unknown, they are replaced by estimates [17],

$$\hat{r}(k) = \frac{1}{N}\sum_{n=k}^{N-1} \mathrm{u}(n)\,\mathrm{u}(n-k). \qquad \text{(Eq 3.18)}$$

The least squares problem in Eq 3.14 is solved for the denominator coefficients. This approach is referred to as the over-determined modified Yule-Walker method [21] or the least squares modified Yule-Walker method [23]. Note that the optimal selection of P is an important and an unknown factor. The variable P is the number of equations used or the length of the correlation function. If $P < N$ then the set of equations is underdetermined and the N coefficients cannot be uniquely determined. If $P=N$, the N coefficients can be uniquely determined. If $P > N$ then the set of equations is over-determined and a least squares solution can be found. After estimating a_i, the roots of the characteristic equation, the system poles are identified as the dominant roots in the frequency band of interest. The s-domain poles are then calculated as

$$s_i = \frac{\ln(z_i)}{T} \qquad i = 1, 2, \ldots, N \qquad \text{(Eq 3.19)}$$

where T is the sampling period and z_i are the z-domain roots of the characteristic equation.

The size of the block of data used has a considerable influence on the estimates determined by the AR block-processing algorithm. In general a larger block size

produces a better estimate of frequency and damping ratio. The standard deviation of frequency and damping ratio estimates with their respective true values decrease as the block size increases. However, the deviation in the damping ratio case is larger than the frequency case [20].

Frequency and damping ratio tracking results using initial weight vector estimates from AR block-processing are discussed in Chapter 5.

3.4.2 LMS Mode Tracking with Previous LMS Estimates

Using the same idea discussed in Section 3.4 the LMS algorithm can be used to track the modes using a weight vector from some time into a previous LMS run instead of a cold start. It is expected that the results using a weight vector from a previous LMS run will be better than the best estimate case using a cold start. The LMS algorithm starts with a weight vector corresponding to an estimate close to the weight vector corresponding to the Wiener solution.

The point worth considering in Section 3.4 is that although the results using the previous estimates from AR block-processing or LMS have a better effect on the tracking ability of the LMS algorithm, it consumes extra computation time as compared to the cold start case. Better initial estimates are critical in reducing the magnitude of initial error in the LMS estimate. However, the selection of the step size parameter is still an important component.

The use of an adaptively changing step size parameter to reduce both the variability of the mode estimate and the convergence time is discussed in Chapter 4.

Chapter 4

Adaptive Step Size Least Mean Squares (ASLMS) Algorithm

The solutions for adaptive algorithms take a time-varying form in non-stationary environments. The minimum point of error of the adaptive algorithm acting in a non-stationary environment is not fixed. Adaptive algorithms hence have the added task of tracking the minimum point first and then tracking the solution around the minimum point. Thus it takes more time for the adaptive algorithm to converge to the actual Wiener solution ($\mathbf{w}_0$) in non-stationary environments than it does for it to converge to the actual Wiener solution in stationary environments. This chapter deals with the construction of a time varying adaptive filter model which converges to the Wiener solution faster than the usual case.

4.1 Constraints of Adaptive Algorithms in Non-stationary Environments

A stochastic process $\mathbf{x}(t)$ describes how statistical properties of an environment vary with time. The time variation in the environment is based on probabilistic laws. The stochastic process is a collection of infinite random variables on each and every time sample t. A stochastic process $\mathbf{x}(t)$ is strictly stationary if its statistical properties are time invariant. Therefore, two samples of the process taken at two different points in time are the same. Let p denote a stochastic process, so that in a strictly stationary process $p(n) = p(n+\alpha)$ where α denotes a time shift [24]. The LMS algorithm is a linear adaptive filtering algorithm with two separate processes, filtering processes and adaptive processes. During the filtering processes, the desired response $d(n)$ and the tap input vector $u(n)$ are used to generate an error vector $e(n)$.

In the adaptive processes, the input vector $\mathbf{u}(n)$ and the error vector $e(n)$ are compared and a correction is applied to the tap weight vector. The scaling parameter used

for this correction is called the step size parameter (μ). The three important equations governing the LMS operation described above are [17]:

$$y(n) = \underline{\mathbf{w}}^{H}(n)\underline{\mathbf{u}}(n-1) \qquad \text{(Eq 4.1)}$$

$$e(n) = \mathrm{u}(n) - y(n) \qquad \text{(Eq 4.2)}$$

$$\underline{\mathbf{w}}(n+1) = \underline{\mathbf{w}}(n) + \mu\underline{\mathbf{u}}(n-1)e^{*}(n) \qquad \text{(Eq 4. 3)}$$

where $\underline{\mathbf{u}}(n\text{-}1) = [\mathrm{u}(n\text{-}1)\ \mathrm{u}(n\text{-}2). \ . \ .\mathrm{u}(n\text{-}\mathrm{M})]^{\mathrm{T}}$ is the input data vector with M past values, $\underline{\mathbf{w}}(n) = [\mathrm{w}_1(n)\ \mathrm{w}_2(n)\ldots.\ \mathrm{w}_{\mathrm{M}}(n)]^{\mathrm{T}}$ is the time varying filter tap weight vector, $y(n)$ is the filter output, $e(n)$ is the error estimate, μ is the step size parameter, and M is the filter order.

The cost for an adaptive filter to control its tap weights can be explained with the help of $J(w)$, a continuously differentiable cost function. The adaptive algorithm has to find an optimal solution $\mathbf{w}_o$ such that the statement of unconstrained optimization $J(\mathbf{w}_o) \leq J(\mathbf{w})$ holds true for all values of the weight vector $\mathbf{w}$. The numerical difference between the final value of the cost function $J(\infty)$ and the minimum value of the cost function $J_{\min}$ is called the excess mean square error $J_{ex}(\infty)$, the cost of the stochastic mechanism to control the tap weights in the LMS filter.

The misadjustment $\mathcal{M}$ is given as

$$\mathcal{M} = \frac{J_{ex}(\infty)}{J_{\min}}. \qquad \text{(Eq 4. 4)}$$

The misadjustment parameter measures the LMS algorithm solution's proximity to the optimal solution. Control of the step size plays an important role in the variability of the estimates and the convergence time of the LMS algorithm in a non-stationary environment. In a stationary environment the minimum cost function J_{min} is fixed, but in a non-stationary environment J_{min} takes a time varying form. Furthermore, due to the presence of a gradient noise in the LMS algorithm, the tap weight vector follows a Brownian movement around the minimum point of error performance rather than converging to the Weiner solution [17]. So the adaptive algorithm has the added task of first having to track the minimum point and then having to track the solution around the minimum point, which makes the adaptive algorithm produce more variable estimates.

4.2 LMS Algorithm in Non-stationary Environments

The operating principle of the LMS algorithm in non-stationary environments is governed by two basic principles:

- First-order Markov process
- Multiple regression.

The unknown dynamic equations of a non-stationary environment are modeled by a filter whose weight vector $\mathbf{w}_o(n)$ undergoes a first order Markov process, given by

$$\mathbf{w}_o(n+1) = a\mathbf{w}_o(n) + \omega(n) \qquad \text{(Eq 4.5)}$$

where $\omega(n)$ is the process noise vector with zero mean and correlation matrix R_ω and a is a parameter close to unity [17]. Thus the tap weight vector $\mathbf{w}_o(n)$ may be assumed to be originating from the process noise $\omega(n)$.

According to the principle of multiple regressions the desired response $d(n)$ of

the filter is given by [17]:

$$d(n) = \mathbf{w}_o^{H}(n)u(n) + v(n) \qquad \text{(Eq 4.6)}$$

where $v(n)$ is the measurement noise with mean zero and variance σ_v^2.

Although $u(n)$ and $v(n)$ are stationary $d(n)$ takes a non-stationary form because of the fact that the minimum point of error $\mathbf{w}_o(n)$ is time-varying in a non-stationary environment. Figure 4.1 shows the linear dynamic model of an adaptive algorithm operating in a non stationary environment.

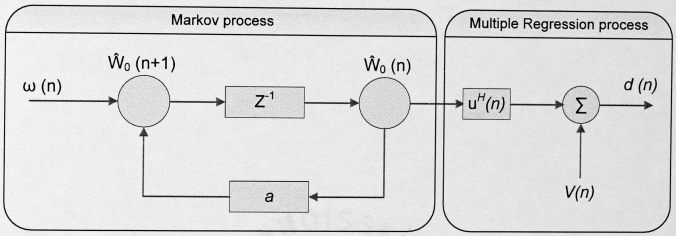

Figure 4.1: Line dynamic model of a non-stationary environment [17].

The error signal under these conditions is are given by

$$e(n) = \mathrm{d}(n) - y(n). \qquad \text{(Eq 4.7)}$$

Substituting Eq 4.6 in Eq 4.7 and expanding $y(n)$ we get

$$e(n) = \mathbf{w}_o^{H}(n)u(n) + v(n) - \mathbf{w}^{H}(n)u(n). \qquad \text{(Eq 4.8)}$$

As, $\mathbf{w}_o(n)$, the target to be tracked by the filter is approached, the tap weight

vector of the adaptive filter at the nth iteration $\mathbf{w}(n) = \mathbf{w}_o(n)$, where $\mathbf{w}_o(n)$ is the final Wiener solution. Eq 4.8 reduces to Eq 4.9

$$e(n) = v(n). \tag{Eq 4.9}$$

Thus, the minimum mean square error produced by the adaptive filter in a non-stationary environment is the irreducible error variance. Figure 4.2 shows the multi regression model incorporated in an adaptive filter to yield an adaptive filter model for use in non-stationary environments.

4.3 Degree of Non-stationarity

The degree of nonstationarity is a quantity that measures the rate of variation of statistics of the non-stationary model. It is denoted by the term 'α' and defined as the square root of the ratio of expectation of the squared magnitude of the inner product of the process noise $\omega(n)$ and vector $u(n)$ to the average power of measurement noise $v(n)$ [17].

$$\alpha = \left(\frac{E\left[\left| \omega^H(n) u(n) \right|^2 \right]}{E\left[\left| v(n) \right|^2 \right]} \right)^{1/2} = \frac{1}{\sigma_v} \left(\left(tr\left[\mathrm{R}_\omega \mathrm{R}_u \right] \right) \right)^{1/2} \tag{Eq 4.10}$$

where R_ω is the correlation matrix of the process noise $\omega(n)$, R_u is the correlation matrix of the vector $u(n)$ and $tr[\ ]$ denotes the trace of the matrix enclosed within the square brackets.

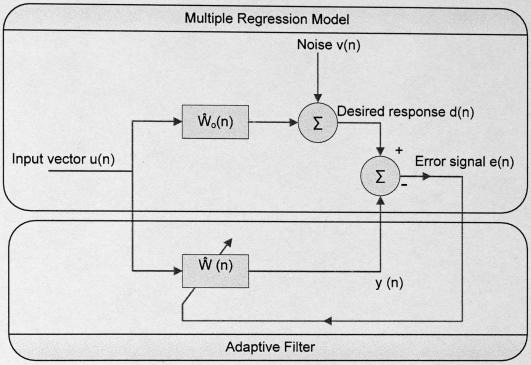

Figure 4.2: Multi regression model incorporated in an adaptive filter for use in non-stationary environments [17].

The following assumptions are made while studying the performance of adaptive algorithms in non-stationary environments [17]:

- The process noise $\omega(n)$ is white with zero mean and correlation matrix R_{ω}.
- The measurement noise $v(n)$ is white with zero mean and variance σ_v^2.
- The process noise and the measurement noise are independent of each other.

In non-stationary environments the misadjustment parameter ($\mathcal{M}$) is related with the degree of nonstationarity α. From Eq 4.9 it is relevant that the minimum mean square error $J_{\min}$ that an adaptive filter can obtain is the irreducible error variance σ_v^2 of the measurement noise $v(n)$. Under the most efficient operating conditions of the adaptive filter in non-stationary environments the error produced $\varepsilon(n)$ will be equal to the process noise $\omega(n)$. By setting the correlation matrix of $\varepsilon(n)$ to be equal to the correlation matrix of $\omega(n)$ we achieve the following [17]:

$$\mathcal{M} = \frac{J_{ex}(\infty)}{J_{\min}} \geq \frac{tr[R_u R_\omega]}{\sigma_v^2} = \alpha^2. \qquad \text{(Eq 4.11)}$$

Thus, the square root of the misadjustment parameter ($\mathcal{M}$) plays an important role in defining the degree of nonstationarity.

From Eq 4.11 two worthy conclusions can be made which serve as the building blocks for the adaptive algorithm that can track time-varying systems:

- 'α' the degree of nonstationarity is small for slow statistical variations, which in turn refers that the misadjustment factor ($\mathcal{M}$) and the step size parameters (μ) are also small.
- For faster statistical variations, α is large and dealing with a α greater than unity refers to a misadjustment that exceeds 100 percent which serves no purpose in building an adaptive algorithm.

In other words, if the degree of nonstationarity is high then the misadjustment factor, which is directly proportional to the square root of the degree of non-stationarity, also increases, which in turn causes the step size parameter also to increase. Thus, the frequency and damping estimates of the adaptive filter designed to work in a non-stationary environment will have more variable results. However, since the step size parameter is inversely proportional to the time constant of the filter, the convergence time of the estimates will decrease substantially.

4.4 Modified LMS Algorithm for Performance in Non-stationary Environments

Based on the assumptions made in the first–order Markov process and the multi regression model analysis with mean square deviation, the excess mean square error

$J_{ex}(n)$ may be expressed as the sum of $J_{ex1}(n)$ and $J_{ex2}(n)$. $J_{ex1}(n)$ is called the estimation noise and is due to the weight vector noise from the multiple regression model and $J_{ex2}(n)$ is called the lag noise and is due to the weight vector noise from the adaptive filter [17]. The lag noise is specifically attributed to the nonstationary environment.

Similarly the misadjustment can be expressed as

$$\mathcal{M}(n) = \mathcal{M}_1(n) + \mathcal{M}_2(n) \qquad \text{(Eq 4.12)}$$

where $\mathcal{M}_1(n)$ is noise misadjustment and $\mathcal{M}_2(n)$ is called the lag misadjustment, which again is specifically attributed to the nonstationary environment. The noise misadjustment varies linearly with the step size parameter μ and the lag misadjustment varies inversely with μ. Thus, in mean square deviation the misadjustment leads to two different values of the step size parameters which emphasize two different aspects of tracking problems. An optimum choice of the step size parameter has to be made in every successive iteration to achieve the best tracking results.

A forth equation is added to the set of three LMS equations (Eq 4.1 - Eq 4.3) to adaptively update the step size parameter [17]:

$$\boldsymbol{\mu}(n) = \boldsymbol{\mu}(n-1) + \rho e(n)\gamma^H(n)\mathbf{u}(n) \qquad \text{(Eq 4.13)}$$

where γ^H is the gradient vector defined as the partial derivative of the weight vector at a sample (iteration) with respect to the step size parameter of the same sample,

$$\gamma(n) = \frac{\partial\, \mathrm{w(n)}}{\partial\, \mu(\mathrm{n})} \qquad \text{(Eq 4.14)}$$

and ρ is a small positive constant which controls the update of the step size parameter. If the gradient vector is included in the update of the step size parameter, the update in step

size during every iteration of the adaptation is reduced. Therefore, the error estimate $e(n)$ during each iteration is reduced and this results in better tracking performance in terms of convergence time. Figure 4.3 shows the block diagram of the ASLMS algorithm.

The weight vectors generated by the ASLMS algorithm give us the information about the modes present in the input power system data $\mathbf{u}(n)$ which are stochastic in nature. The roots of the z-domain polynomial are calculated from the weight vector which is then converted into the s-plane. The z-domain polynomial is given by:

$$a(z,n) = 1 - \mathrm{w}_1(n)z^{-1} - \ldots \mathrm{w}_M(n)z^{-M}. \qquad \text{(Eq 4.15)}$$

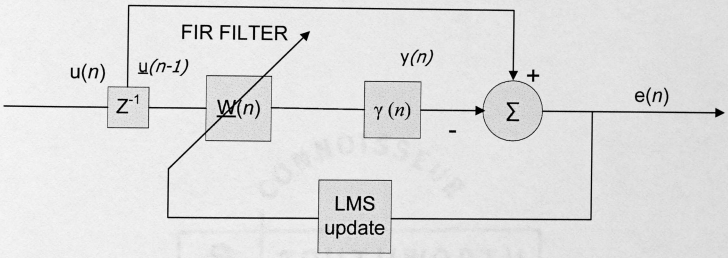

Figure 4.3: Block diagram of ASLMS algorithm [17].

Conversion to the s-plane is performed by implementing

$$s(n) = \ln(roots(a(z,n))) / \mathrm{T} \qquad \text{(Eq 4.16)}$$

where T is the sampling period. The total number of roots will be equal to the filter tap length *M*. The roots calculated contain the information about the frequency and damping ratio of the dominant mode.

For non-stationary data and a small μ, the LMS algorithm will converge if [17]:

$$0 < \mu < (2 / total\ MSV) \qquad \text{(Eq 4.17)}$$

where MSV is the mean-square value given by the relation

$$total\ MSV = \frac{M}{L}\sum_{n=0}^{L-1} u^2(n) \qquad \text{(Eq 4.18)}$$

where L is the length of the input data and M represents the number of tap weights of the filter.

The difference between the LMS and the ASLMS algorithm is in Eq 4.13 where the step size is updated every iteration. This step allows the ASLMS algorithm to track the minimum point of error in less time than an LMS algorithm. The time of convergence of an estimate tracked by the ASLMS algorithm is far less than the time taken by the LMS algorithm. Due to the presence of σ_v, the irreducible error variance, the tracking of the estimate is more variable using the ASLMS algorithm. The LMS and ASLMS estimates of frequency and damping ratio on the power system data from line 17 between buses 22 and 26 of the simulated system are discussed in Chapter 5.

Chapter 5

Application of LMS Algorithm, Combination Algorithms and ASLMS Algorithm on Test System Data

The mode estimation techniques were applied to the simulated 19-machine test system data. The results from the LMS algorithm with a cold start, LMS algorithm with initial estimates from AR block-processing, LMS algorithm with initial estimates from the previous LMS run, and ASLMS algorithm were examined for the stationary mode at 0.2624 Hz. The data were obtained from line 17 of the 19-machine system discussed in Chapter 2.

5.1 LMS Results with a Cold Start

The 0.26 Hz mode with a frequency of 0.2624 Hz and damping ratio of 10.33 %, the dominant mode found in the western North American power grid, was of interest in this work. The mode was first tracked over time using the LMS algorithm. The LMS algorithm was started with zero initial weight vectors (cold start). The LMS algorithm was applied to the same data window using three different step size parameters to start with. The three different values of step size parameter (μ) used were 7.8231 e-04, 3.5566 e-04 and 1.4224 e-04. Figure 5.1 and Figure 5.2 represent the LMS estimate of frequency and damping ratio versus time, respectively, for the simulated 19-machine data. At this point it is noteworthy that the step size parameter of the LMS filter is inversely proportional to the average time constant (Γ_{avg})

$$\mu \propto \frac{1}{\Gamma_{avg}}. \qquad \text{(Eq 5.1)}$$

Figures 5.1 and 5.2 show that as the value of μ decreases the variability decreases since a majority of the gradient noise in the LMS estimates is filtered by a large Γ_{avg}.

However, if the step size is further reduced to get less variable results, the convergence time increases. Since the weight vector used is initially zero, the LMS algorithm takes more time to converge to the actual values of frequency and damping ratio.

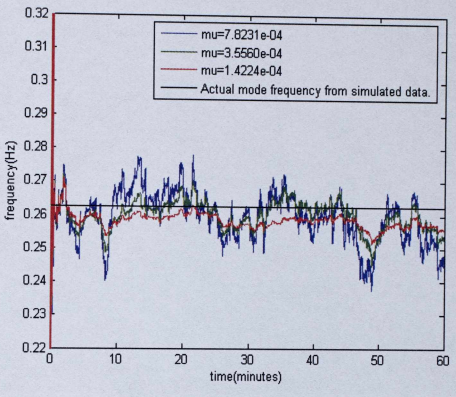

Figure 5.1: Mode frequency vs. time for the megawatt data between buses 22 and 26 of the 19-machine system. (60 minutes, cold start and μ = 7.8231 e-04, 3.5560 e-04 and 1.4224 e-04).

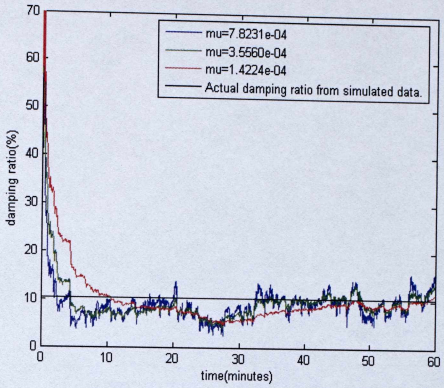

Figure 5.2: Damping ratio vs. time for the megawatt data between buses 22 and 26 of the 19-machine system. (60 minutes, cold start and μ = 7.8231 e-04, 3.5566 e-04 and 1.4224 e-04).

5.1.1 LMS Results with Previous Estimates from AR Block-processing

The LMS algorithm was reapplied to the same data set using an initial weight vector estimate from the AR block-processing technique for five different values of block sizes. Figure 5.3 and Figure 5.4 show the LMS estimate of frequency and damping ratio versus time, respectively, using an initial weight vector estimate from the AR block-processing technique for different block sizes and a step size ten times smaller than the best estimate case with a cold start LMS (3.5560 e-04). A decrease in variability of the mode estimate can be observed using an initial weight vector estimate from the AR block-processing technique with a ten times smaller step size parameter. The standard deviation of the frequency estimates with the actual mode frequency (0.2624 Hz) decreases with the increase in block size. These results agree with the results presented in [20]. Similar results were observed with the damping ratio estimates.

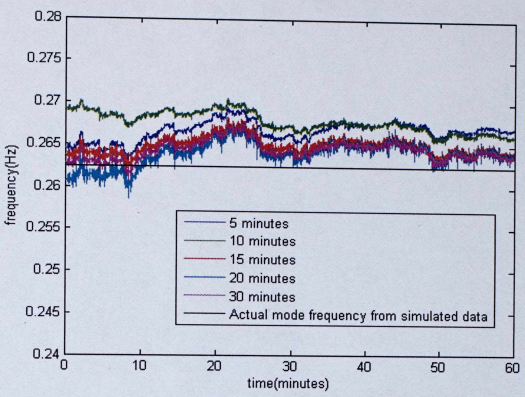

Figure 5.3: Mode frequency vs. time for the megawatt data from the 19-machine system between buses 22 and 26 of the 19-machine system. (60 minutes, $\mu = 3.556$ e-05, weight vector from AR for different block sizes).

The LMS algorithm was then reapplied to the same data set using an initial weight vector from the LMS algorithm 10 minutes into the previous LMS run. The step size parameter used was reduced by a factor of 10 from the best estimate case with a cold start. Figure 5.5 and Figure 5.6 show the comparison of LMS estimates with mode frequency and damping ratio, respectively, using a cold start, using an initial weight vector from 10 minutes into the previous LMS run and an initial weight vector from AR block-processing with a 10 minute block size. The step size was reduced by a factor of 10 compared to the best LMS estimates with the cold start case. Using an initial weight vector estimate from another algorithm allows the LMS algorithm to converge to the actual value with much less variability in the running estimate.

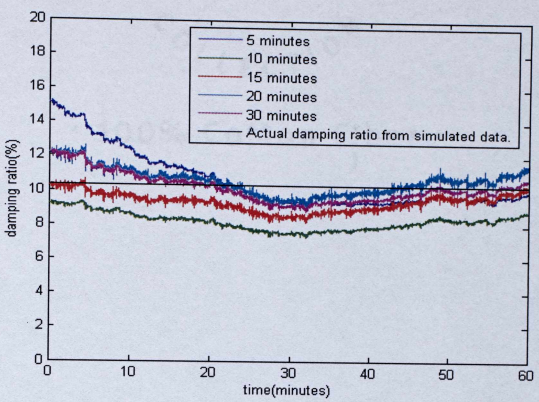

Figure 5.4: Damping ratio vs. time for the megawatt data of the 19-machine system between buses 22 and 26 of the 19-machine system. (60 minutes and μ = 3.556 e-05, weight vector from AR for different block sizes).

The accuracy of frequency estimates using the initial weight vector estimate from AR block-processing is similar to that of the frequency estimate using the initial weight vector from the previous LMS run. However, the frequency estimates using an initial weight vector from AR block-processing tend to move towards the actual estimate, unlike the frequency estimate case using an initial weight vector from 10 minutes into the previous LMS algorithm.

Comparing the damping ratio estimates, the estimates using an initial weight vector from AR block-processing are closer to the actual damping ratio from simulated data than the estimates using an initial weight vector from the previous LMS estimates.

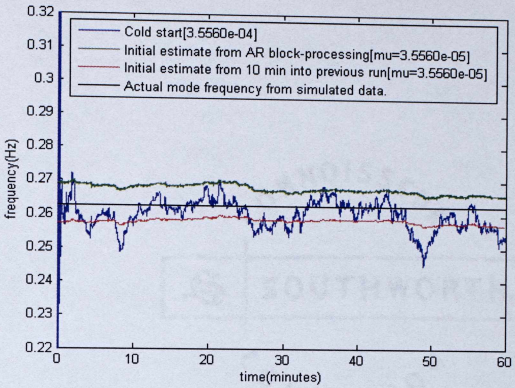

Figure 5.5: Mode frequency vs. time by cold start for the megawatt data of the 19-machine system between buses 22 and 26 of the 19-machine system, initial estimate from 10 minutes run into previous LMS run and initial weight vector from AR block-processing.

Using initial weight vector estimates from other algorithms has helped the LMS algorithm in converging faster with less variability compared to the cold start case. However, as mentioned earlier in Chapter 3, these techniques consume extra computation time as compared to the cold start case because of combining two algorithms. Quicker convergence and less variable results can be obtained by using the ASLMS algorithm discussed in the following section.

5.2 Results from ASLMS Algorithm

The ASLMS algorithm is applied to the power system data for mode estimation with the assumption that the data is non-stationary. The degree of non-stationarity (α) has an important effect on the performance of non-stationary environments.

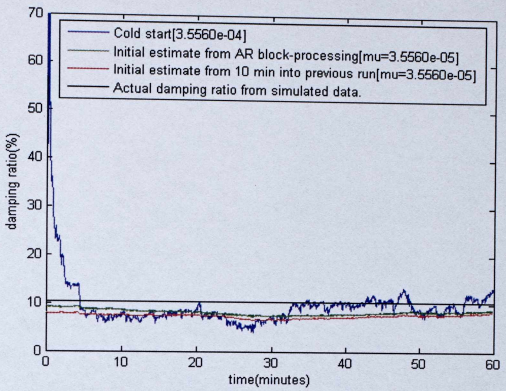

Figure 5.6: Damping ratio vs. time using cold start for the megawatt data of the 19-machine system between buses 22 and 26 of the 19-machine system, initial estimate from 10 minutes into previous LMS run and initial weight vector from AR block-processing.

The square root of the misadjustment parameter ($\mathcal{M}$) places an upper bound on the degree of non-stationarity [17]. If the value of α is greater than unity, misadjustment produced by the adaptive filter is greater than 100 %. For a misadjustment of greater than 100 % no advantage can be gained by building an adaptive filter for tracking in a non-stationary environment. The degree of non-stationarity of the 19-machine simulated data between buses 22 and 26 was calculated to be 0.4831. The minimum misadjustment that can be achieved by the ASLMS filter over the simulated data set is the square root of the degree of non-stationarity (minimum $\mathcal{M}$=0.233).

The Least Mean Squares (LMS) and the Adaptive Step Size Least Mean Squares (ASLMS) algorithm were reapplied to the simulated data to track the dominant mode as in the previous sections. The ASLMS algorithm results in faster convergence; hence the

step size parameter was reduced by a factor of 50 to achieve less variable estimates. Figures 5.7 and 5.8 represent the estimates of frequency and damping ratio, respectively, by the LMS and the ASLMS algorithms with a zero initial weight vector (cold start). The reduced step size parameter used was 7.8231 e-06.

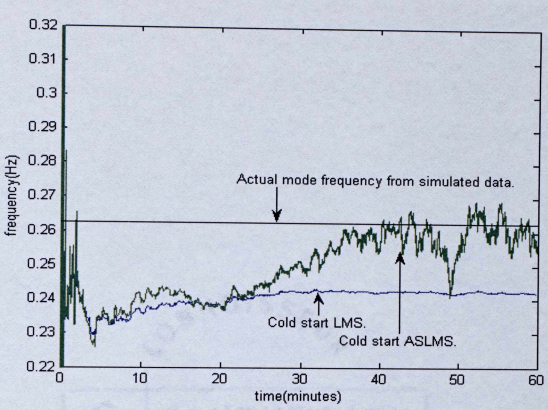

Figure 5.7: Mode frequency vs. time for megawatt data of the 19-machine system between buses 22 and 26 of the 19-machine system (60 minutes, cold start, LMS: μ=7.8231 e-06, ASLMS: μ=7.8231 e-06, ρ= 1.8182 e-03).

The ASLMS algorithm performs well in terms of time of convergence. The ASLMS estimates converge in almost half the time taken by the LMS estimates to converge to the actual value. This holds for both the frequency and damping ratio estimates. The increased variability in the ASLMS estimates is due to the presence of the lag noise J_{ex2} and the irreducible error variance, σ_v described in Chapter 4. The small positive constant ρ which controls the adaptation of the step size parameter in the ASLMS algorithm was set to 1.8182 e-03 for the frequency estimates in Figure 5.7 and 1.428 e-03 for the damping ratio estimates in Figure 5.8.

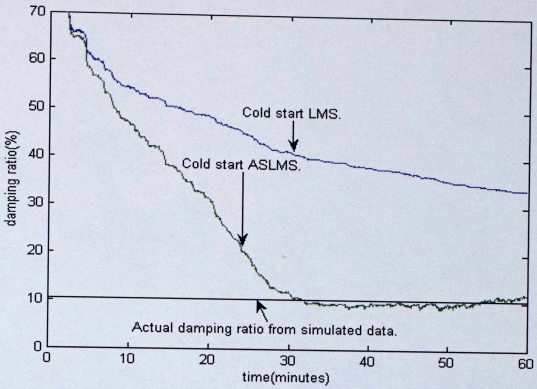

Figure 5.8: Damping ratio vs. time for megawatt data of the 19-machine system between buses 22 and 26 of the 19-machine system (60 minutes, cold start, LMS: μ=7.8231 e-06, ASLMS: μ=7.8231 e-06, ρ= 1.00 e-03).

The selection of the small positive constant ρ plays an important role in controlling the adaptation and convergence of the ASLMS estimates. From Eq 4.13 it was observed that

$$\rho \propto \mu. \qquad \text{(Eq 5.2)}$$

The mode frequency was estimated over time by the ASLMS algorithm using a cold start with three different values of ρ (3.33 e-03, 1.82 e-03 and 1.00 e-03) to illustrate the importance of the small positive constant in the adaptation of the ASLMS algorithm. Similarly, the damping ratio was estimated over time using a cold start ASLMS algorithm with three different values of ρ (6.67 e-03, 1.43 e-03 and 7.14 e-04). The step size parameter used to start the ASLMS algorithm was set to 7.8231 e-06 for all the cases mentioned above. Figures 5.9 and 5.10 show the ASLMS estimate of frequency

and damping ratio, respectively, versus time with a zero initial weight vector for three different values of ρ.

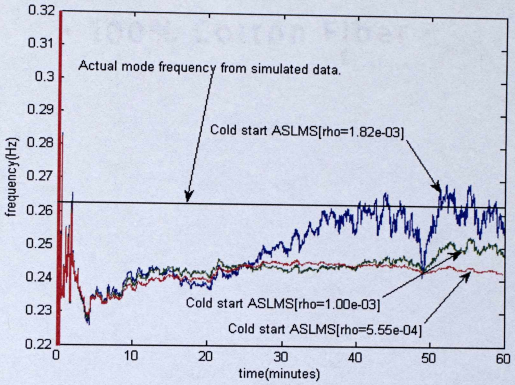

Figure 5.9: Mode frequency vs. time for the 19-machine megawatt data between buses 22 and 26 of the 19-machine system (60 minutes, cold start, μ=7.8231 e-06, ρ=1.82 e-03, 1.00 e-03, 5.55 e-04).

If ρ is reduced to very small values like 5.53 e-04 and 2.85 e-04 in the frequency and damping ratio estimates, respectively, the estimates behave like ordinary LMS estimates with a cold start. Figures 5.7, 5.8, 5.9 and 5.10 show that the estimates from the ASLMS algorithm take less time to converge to the actual value. The variability of the estimates from the ASLMS algorithm is, however, more than the estimates from the LMS algorithm for the same value of the step size parameter.

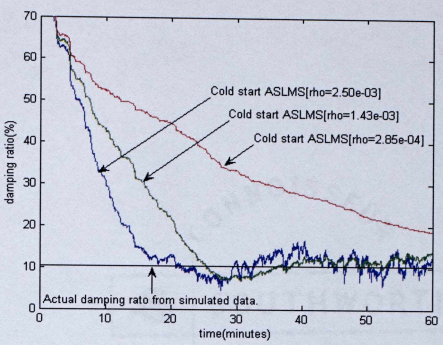

Figure 5.10: Damping ratio vs. time for the 19-machine megawatt data between buses 22 and 26 of the 19-machine system (60 minutes, cold start, μ=7.8231 e-06, ρ=2.50 e-03, 1.43 e-03, 2.85 e-04).

To achieve both quicker time of convergence and less variable estimates the following three combinations were studied:

- Case 1: The LMS algorithm was reapplied to the same data set using an initial weight vector estimate 10 minutes into the previous LMS estimates (LMS-LMS).
- Case 2: The ASLMS algorithm was reapplied to the same data set using an initial weight vector estimate 10 minutes into the previous LMS estimates (LMS-ASLMS).
- Case 3: The LMS algorithm was reapplied to the same data set using an initial weight vector estimate 10 minutes into the previous ASLMS estimates (ASLMS-LMS).

The step size was further reduced by a factor of ten (7.8231 e-07) to help decrease the variability in the mode estimates. Figures 5.11 and 5.12 show the estimates of

frequency and damping ratio for the three cases mentioned earlier. The step size parameter used was the lowest that could be used, since further reduction in step size gave rise to convergence time constraints.

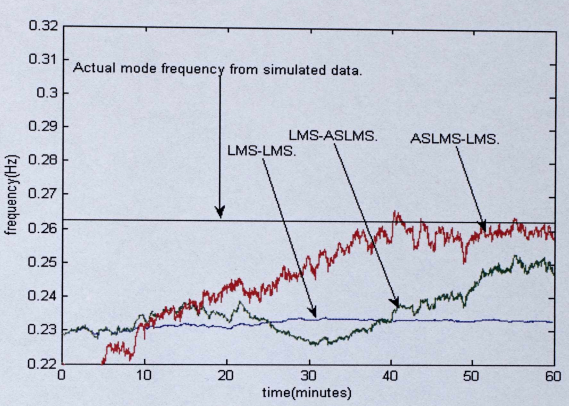

Figure 5.11: Mode frequency vs. time for megawatt data of the 19-machine system between buses 22 and 26 (60 minutes, μ=7.8231 e-07, LMS-ASLMS: ρ=2.00 e-03, ASLMS-LMS: ρ=5.71 e-03).

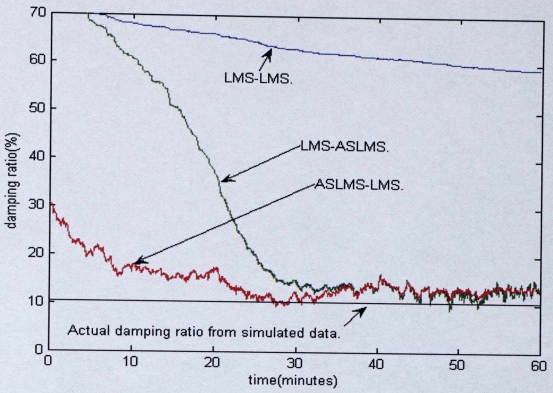

Figure 5.12: Damping ratio vs. time for megawatt data of the 19-machine system between buses 22 and 26 (60 minutes, μ =7.8231 e-07, LMS-ASLMS: ρ =2.00 e-03, ASLMS-LMS: ρ =5.00 e-03).

From Figures 5.11 and 5.12 it is clear that the weight vector from the previous ASLMS estimates (case 3) gives better results compared to the weight vector from previous LMS estimates (case 2) . The figures also show that, using previous ASLMS estimates in the LMS algorithm gives more accurate estimates than using previous LMS estimates.

5.3 Error Tracking (ET) Algorithm

The selection of the step size parameter is the most important condition to be satisfied in achieving an accurate tracking result. The reduction in the step size parameter removes a majority of the gradient noise and hence reduces the variability of the estimates. However, the time of convergence increases. Several techniques were employed to reduce the time of convergence of the frequency and damping ratio

estimates. Previous estimates from LMS and AR reduce the time of convergence, but consume more computation time. The ASLMS algorithm reduces the time of convergence by a considerable amount. However, the estimates are variable and consume more computation time.

The Error Tracking (ET) algorithm combines the fast convergence capability of the ASLMS algorithm and less variable estimates of the LMS algorithm and thus achieves quicker convergence of estimates with much less variability. The ET algorithm works on the value of the estimate error in the adaptive filter. The ET algorithm starts with a cold start ASLMS algorithm with a very high ρ for faster convergence. As the value of the estimation error decreases and the mode estimates fall between 99% and 101% of the actual value, the ET algorithm switches computation methods from the ASLMS to the LMS algorithm with a 10 times reduced step size for less variable results. Figure 5.13 and 5.14 show the frequency and damping ratio estimates of the ET algorithm. The ET algorithm also switches back from the LMS algorithm to the ASLMS algorithm if the estimates fall below 99 % or move above 101% of the actual mode value. Figures 5.13 and 5.14 show the mode estimates of the ASLMS algorithm in blue, the mode estimates of the LMS algorithm with a 10 times reduced step size in red and the actual mode estimates in black. Figure 5.13 shows that as soon as the frequency estimates of the ASLMS algorithm (shown in blue) fall between 99% and 101% of the actual mode frequency from the simulated system (shown in black), the ET algorithm switches computation from the ASLMS algorithm to the LMS algorithm and tracks the mode frequency using the LMS algorithm (shown in red) with a ten times reduced step size. The higher the value of the small positive constant used to start the ASLMS algorithm the quicker the ET estimates will fall within $\pm$ 1% of the actual value.

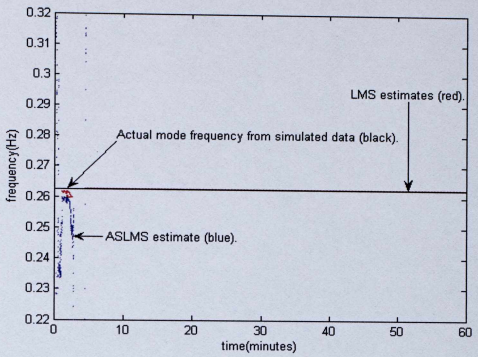

Figure 5.13: Mode frequency vs. time for megawatt data between buses 22 and 26 of the 19-machine system (60 minutes, cold ASLMS start ASLMS: μ=7.8231 e-07, ρ=0.04 and LMS: μ=7.8231 e-08).

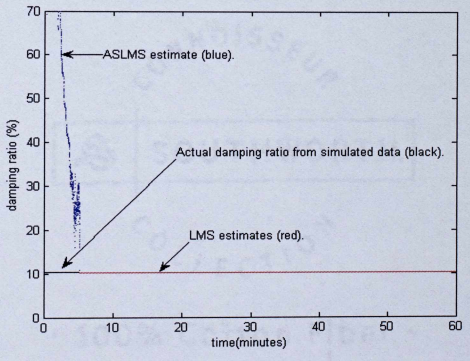

Figure 5.14: Damping ratio vs. time for megawatt data between buses 22 and 26 of the 19-machine system (60 minutes, cold ASLMS start ASLMS: μ=7.8231 e-07, ρ=0.02 and LMS: μ=7.8231 e-08).

The LMS and ASLMS estimates of frequency and damping ratio using the June 2000 and June 2005 ambient power system data collected from monitors in the western US grid are discussed in Chapter 5.

Chapter 6

Application of LMS Algorithm, Combination Algorithms and ASLMS Algorithm on Ambient Power System Data

The behavior of mode estimation techniques on the simulated data were studied in Chapter 5. The same techniques were applied to ambient power system megawatt data in this chapter. Two sets of ambient power system data were used to check the consistency of the algorithms in estimating the electromechanical modes. The first data set used was the smaller of the two, consisting of 18 minutes of real power flow on June 7, 2000 from Malin-Round Mountain #1 (MR #1). The second and the longer data used was 180 minutes of real power flow on June 13, 2005 from MR #1. The idea behind using two data sets of different sizes was to check if the algorithms could estimate the modes quickly (under 18 minutes–shorter data) and also be consistent in tracking the converged result for a longer data set. Also, the degree of non-stationarity of the two data blocks varied. Table 6.1 shows the calculated degree of non-stationarity of the June 7, 2000 and June 13, 2005 data.

Table 6.1: Degree of non-stationarity of ambient data sets

Degree of non-stationarity	**June 2000 MR #1 data.** (after re-sampling)	**June 2000 MR #1 data.** (before re-sampling)	**June 2005 MR #1 data.**
α	0.3332	0.3429	0.8867

The June 7, 2000 data were re-sampled from 5652 samples to 54000 samples for comparison with the June 13, 2005 data of 54000 samples (3 hours). The resampling was achieved by using the resample function in MATLAB®. The resample function applies an anti-aliasing (lowpass) FIR filter to the data to be resampled. During the resampling process, it compensates for the filter's delay. Resampling of the shorter data set to the size

of the larger data set was done to achieve an un-biased comparison of the degrees of non-stationarity of the two data sets. However, Table 6.1 shows that the re-sampling did not have a considerable effect on the degree of non-stationarity of the data set.

6.1 Estimating Electromechanical Modes in June 7, 2000, MR #1 Ambient Data.

The algorithms were applied to the pre-processed ambient data from MR #1 at the California-Oregon inter-tie. Figure 6.1 shows one minute of pre-processed real power flow of MR #1 data from June 7, 2000. The collected data were decimated from 20 samples/second to 5 samples/second for the reasons mentioned in Chapter 2.

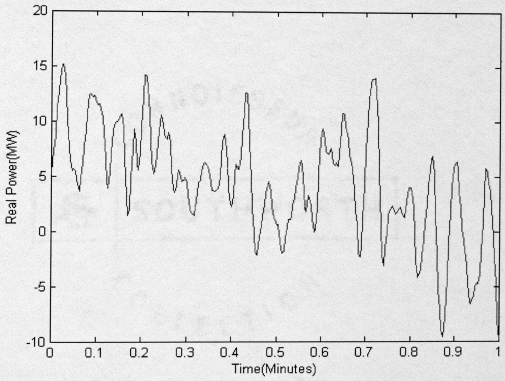

Figure 6.1: One-minute of preprocessed megawatt data from Malin-Round Mountain #1 on June 7, 2000 (Time Reference: 14:28:05 PM PST).

6.1.1 Dominant Mode Identification using Auto-Regressive Block-processing

Unlike the simulated 19-machine test system data used in the previous chapter the information regarding the exact location and strength of the dominant mode was not available. The auto-regressive (AR) block-processing technique was applied to the data to identify the dominant mode frequency and damping ratio. Different block sizes of 5, 10, 15, 18 and 18.84 (full data block) minutes were used in the AR block-processing technique. The AR estimates for mode frequency and damping ratio are listed in Table 6.2 for different block sizes. Several correlation lengths (K) and number of poles (N) were tested using AR block-processing, but the best results were obtained using K=57 and N=30. Using AR block-processing the number of zeros in the system (M) was set to 0.

Table 6.2: Frequency and percent damping ratio estimates using AR block-processing of MR #1-2000 data

Block Size (Minutes)	Frequency (Hertz)	Damping Ratio (%)
5	0.2681	8.225
10	0.2754	8.775
15	0.2753	8.176
18	0.2728	7.824
18.85 (full data)	0.2723	7.884

6.1.2 LMS Results with a Cold Start

The LMS algorithm with a zero initial weight vector (cold start) was applied to the 18.85 minutes of data to estimate the dominant mode frequency and damping ratio of the 0.2728 Hz and 7.884%. The AR estimates using the full block of data were used for comparison purposes with the estimates from the LMS algorithm. Figures 6.2 and 6.3 show the frequency and damping ratio estimates from the cold start LMS algorithm using three different values of step size (μ). The LMS algorithm is expected to exhibit consistency in performance in using the ambient data, as with the simulated data for the decreasing values of step size. As the value of the step size parameter (μ) decreases the variability in the estimate decreases while the time of converge increases.

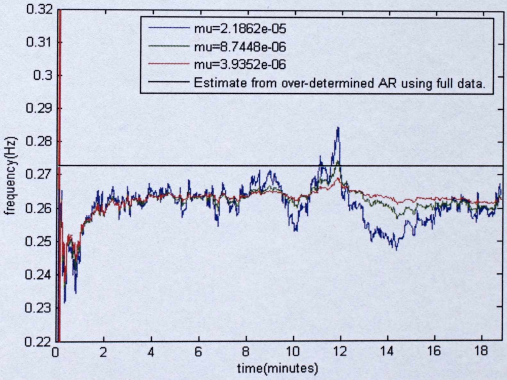

Figure 6.2: Mode frequency vs. time of MR #1, June 7, 2000 data (cold start: μ = 2.1862 e-05, 8.7448 e-06 and 3.9352 e-06).

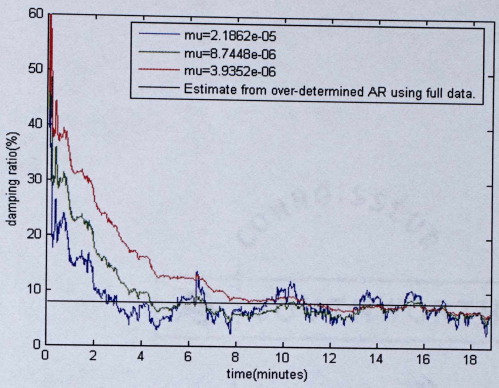

Figure 6.3: Mode damping ratio vs. time of MR #1, June 7, 2000 data (cold start: μ= 2.1862 e-05, 8.7448 e-06 and 3.9352 e-06).

6.1.3 LMS Results with Previous Estimates from AR Block-processing

Figures 6.2 and 6.3 show that the LMS algorithm with a cold start takes more time to converge to the mode estimates indicated by the AR block-processing. The LMS algorithm was reapplied to the same data set using initial mode estimates from AR block-processing with different block sizes as listed in Table 6.2. Reduction in variability of the mode estimate and the convergence time is expected using initial AR estimates in the LMS algorithm. Figure 6.4 and 6.5 show the comparison of frequency and damping ratio estimates, respectively, using the initial estimate from AR for different block sizes with the step size reduced by a factor of 10 compared to the cold start LMS case. The step size was reduced to achieve a decrease in the variability in the estimates. The LMS mode estimates for both frequency and damping ratio approach the AR estimate as the block size used for the AR estimate increases. However, it should be noted that since the AR

estimate using the full block of data is used for comparison purposes with the LMS estimates using initial weight vectors from AR block-processing for different block sizes, the LMS estimate will approach the AR estimate using the full block of data as the AR estimate block size used for initial estimates increases.

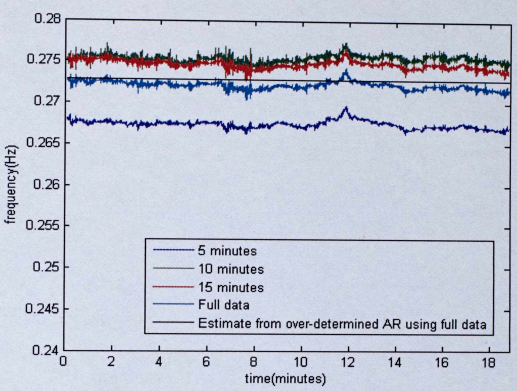

Figure 6.4: Mode frequency vs. time of MR #1, June 7, 2000 data (18.84 minutes, μ = 8.7448 e-07, weight vector from AR for different block sizes).

The initial estimates from AR block-processing help the LMS estimates to achieve reduced variability and convergence time. The reduction in step size compared to the cold start LMS case has reduced the variability of the LMS estimates. The use of initial weight vector estimates from AR block-processing has reduced the variability of the LMS estimates. These results hold for both the frequency and damping ratio cases.

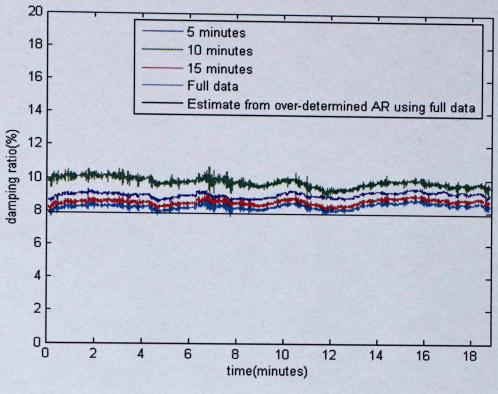

Figure 6.5: Mode damping ratio vs. time of MR #1, June 7, 2000 data (18.84 minutes, μ = 8.7448 e-07, weight vector from AR for different block sizes).

The LMS algorithm was reapplied to the same data block using initial weight vector estimates from 10 minutes into the previous LMS run. The step size parameter was reduced by a factor of 10 compared to the cold start LMS case. Figures 6.6 and 6.7 show a comparison of LMS estimates for mode frequency and damping ratio, respectively, using a cold start LMS, using an initial weight vector from 10 minutes into previous LMS run, and using an initial weight vector from AR block-processing with a 10 minute block size.

Using an initial weight vector from AR block-processing resulted in better initial and sample-by-sample LMS estimates than using estimates from previous cold start applications of the LMS technique. Furthermore, the time of convergence in estimating both the frequency and the damping ratio was less when initial weight vector estimates from the AR block-processing algorithm were used. However, as discussed in the previous chapter, the combinations of algorithms require more computation time compared to the cold start LMS case.

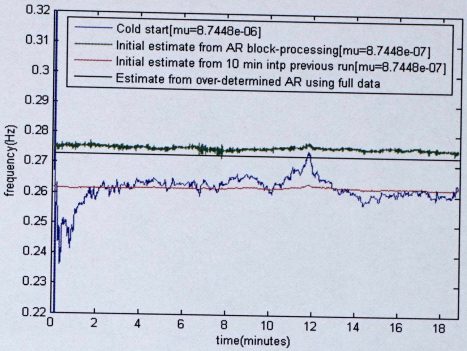

Figure 6.6: Mode frequency vs. time using cold start, using an initial weight vector from 10 minutes into the previous run, and using an initial weight vector from AR block-processing with a 10 minute block size of MR #1, June 7, 2000 data.

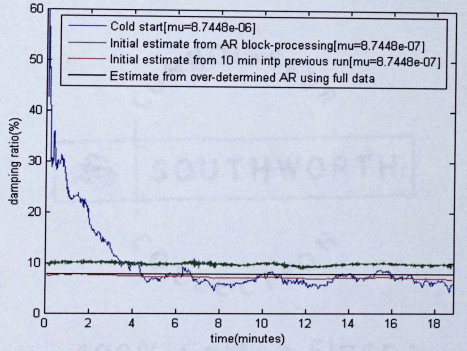

Figure 6.7: Mode damping ratio vs. time using cold start, using an initial weight vector from 10 minutes into the previous run, and using an initial weight vector from AR block-processing with a 10 minute block size of MR #1, June 7, 2000 data.

6.1.4 Results from ASLMS Algorithm

The 0.2723 Hz mode with a damping ratio of 7.372 % was set to be tracked by the ASLMS algorithm. As discussed in Chapter 1, the damping ratio measures the stability of a power system. The higher the damping ratio in the system, the more stable it is. A damping ratio as low as the case under consideration (7.372%) represents that the power system is less stable compared to a system with a damping ratio of 10.33 % (simulated data). The lower damping ratio, and hence lower stability, is a direct consequence of heavy load modulations which show up as noise in the data.

Figures 6.8 and 6.9 represent the estimates of frequency and damping ratios, respectively, using the LMS and the ASLMS algorithms with a cold start. The values of step size parameter μ used in these algorithms was set to 8.7448 e-07. The small positive constant ρ was set to 6.67 e-06 for the frequency estimate in Figure 6.8 and 2.00 e-06 in the damping ratio estimate in Figure 6.9. In terms of convergence time of the estimates the ASLMS algorithm performs far better than the LMS algorithm. The ASLMS algorithm converges to the AR estimates in both the frequency and damping ratio cases, while the LMS estimates of frequency and damping ratio do not converge to the AR estimates after tracking the full length of data. As discussed in Chapter 5, the small positive constant ρ plays an important role in the convergence behavior of the ASLMS estimates. As the small positive constant ρ increases, the convergence time of the estimate decreases while the variability of the estimate increases.

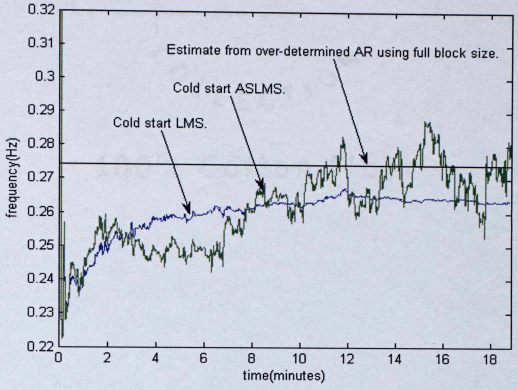

Figure 6.8: Mode frequency vs. time for MR #1, June 7, 2000 data. (18.85 minutes, cold start, LMS: μ=8.7448 e-07, ASLMS: μ=8.7448 e-07, ρ = 6.67 e-06).

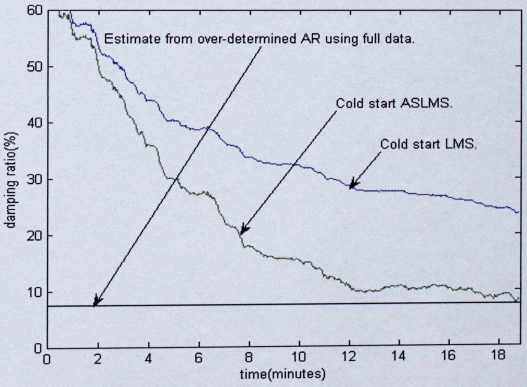

Figure 6.9: Damping ratio vs. time for MR #1, June 7, 2000 data (18.85 minutes, cold start, LMS: μ=8.7448 e-07, ASLMS: μ=8.7448 e-07, ρ = 2.00 e-06).

Figures 6.10 and 6.11 show the mode frequency and damping ratio estimates over time, respectively, from the ASLMS algorithm for different values of ρ. The mode frequency was estimated over time in Figure 6.10 using the ASLMS algorithm with a cold start for three different values of ρ (6.67 e-06, 4.44 e-06 and 1.00 e-06). Similarly, the damping ratio was estimated over time in Figure 6.11 using the ASLMS algorithm, with a cold start for three different values of ρ (1.00 e-05, 6.67 e-06 and 5.00 e-07).

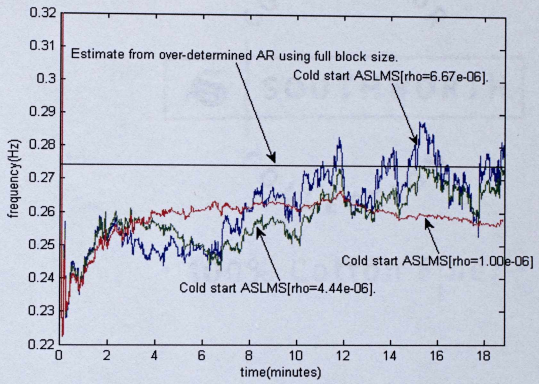

Figure 6.10: Mode frequency vs. time for MR #1, June 7, 2000 data (18.85 minutes, cold start, μ=8.7448 e-07 and ρ=1.00 e-05, 6.67 e-06, 4.00 e-06).

To achieve both quicker time of convergence and less variable estimates the following three combinations were studied:

- Case 1: The LMS algorithm was reapplied to the same data set using an initial weight vector estimate 10 minutes into the previous LMS estimates (LMS-LMS).
- Case 2: The ASLMS algorithm was reapplied to the same data set using an initial weight vector estimate 10 minutes into the previous LMS estimates

(LMS-ASLMS).

- Case 3: The LMS algorithm was reapplied to the same data set using an initial weight vector estimate 10 minutes into the previous ASLMS estimates (ASLMS-LMS).

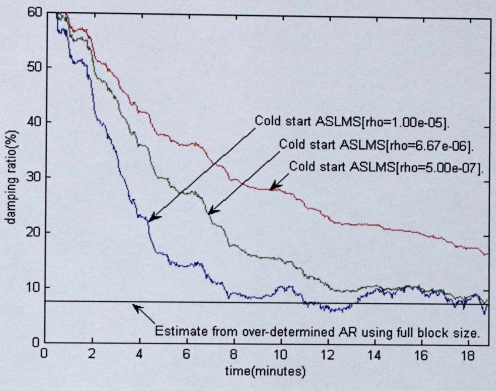

Figure 6.11: Damping ratio vs. time for MR #1, June 7, 2000 data (18.85 minutes, cold start, μ=8.7448 e-07 and ρ=5.00 e-06, 2.00 e-06, 1.42 e-06).

The step size parameter was reduced by a factor of 10 (8.7448 e-08) and was used in all the three cases mentioned above. Figures 6.12 and 6.13 show the mode frequency and damping ratio, respectively, for the three cases mentioned above. The values of ρ used in case 2 and case 3 were 1.33 e-06 and 6.67 e-03, respectively, for the frequency estimates. The values of ρ used in the damping ratio estimates for case 2 and case 3 were 8.33 e-06 and 1.42 e-05, respectively.

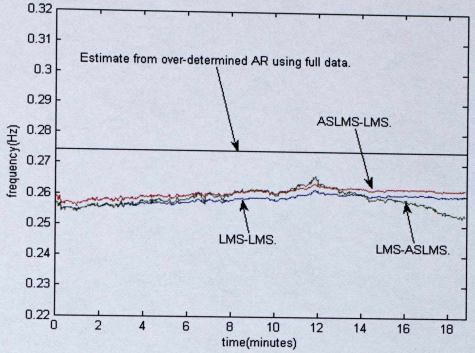

Figure 6.12: Mode frequency vs. time for MR #1, June 7, 2000 data (18.85 minutes, μ=8.7448 e-08, LMS-ASLMS: ρ=1.33 e-06 ASLMS-LMS: ρ=6.67 e-06).

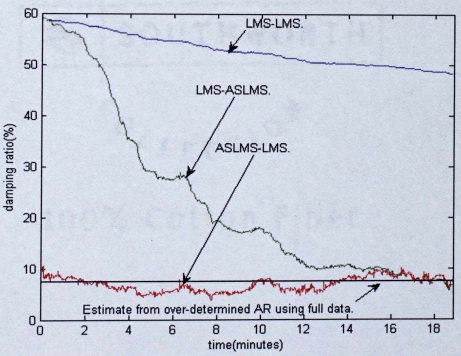

Figure 6.13: Damping ratio vs. time for MR #1, June 7, 2000 data (18.85 minutes, μ=8.7448 e-08, LMS-ASLMS: ρ=8.33 e-06, ASLMS-LMS: ρ=1.42 e-05).

Figures 6.12 and 6.13 show that the ASLMS-LMS case gives better results than the LMS-ASLMS and the LMS-LMS cases. The error variance inherent in the ASLMS algorithm does not have a considerable effect on the damping ratio estimates. Using an initial estimate from the ASLMS algorithm in the LMS algorithm helps to achieve both faster convergence and less variability compared to case 2, where an initial estimate from the LMS algorithm is used in the ASLMS algorithm.

6.2 Estimating Electromechanical Modes in June 13, 2005 MR #1 Ambient Data

The algorithms were reapplied to the longer data set to check the performance of the algorithm over a longer period. The data used were pre-processed ambient data from MR #1 at the California-Oregon inter-tie on June 13, 2005. Figure 6.14 shows one minute of pre-processed real power flow from MR #1 on June 13, 2005. The data were decimated from 20 samples/second to 5 samples/second during pre-processing.

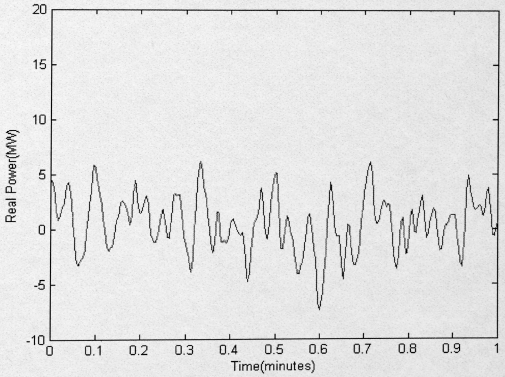

Figure 6.14: One-minute of preprocessed megawatt data from Malin-Round Mountain #1 on June 13, 2005. (Time Reference: 06:00:15 AM PST).

6.2.1 Results from AR Block-processing

The standard deviation of the AR estimates reduces as the block size increases [20]. So for accurate estimates of dominant mode frequency and damping ratio AR block-processing was applied to the whole 48 hours of data. The different block sizes used were 0.25 (15 minutes), 0.5 (30 minutes), 1, 3, 5, 10, 24, 35 and 48 (full data block) hours. A correlation length of K=57 was used. The number of poles (N) and the number of zeros (M) were set to 30 and 0, respectively. Table 6.3 lists the AR estimates of frequency and damping ratio for different block sizes.

Table 6.3: Frequency and percent damping ratio estimates using AR block-processing of MR #1-2005 data

Block Size (Hours)	Frequency (Hertz)	Damping Ratio (%)
0.25 (15 minutes)	0.2622	49.12
0.50 (30 minutes)	0.2559	10.038
1	0.2534	8.481
3	0.2504	9.611
5	0.2535	11.11
10	0.2500	9.94
24	0.2561	11.65
35	0.2499	11.83
48 (full data block)	0.2540	12.12

6.2.2 LMS Results with Cold Start

The LMS algorithm with a zero initial weight vector (cold start) was used to estimate the mode frequency and damping ratio. The standard deviation of frequency and damping ratio estimates from block-processing algorithms decreases as the block size used increases [20]. The AR estimates of frequency and damping ratio for a block size of 48 hours have higher possible accuracy than other block sizes. The AR estimates using the full block of data (48 hours) were used for comparison purposes with the LMS estimates for 180 minutes of data. Figures 6.15 and 6.16 show the LMS estimates of mode frequency and damping ratio, respectively, for three different values of the step size parameter.

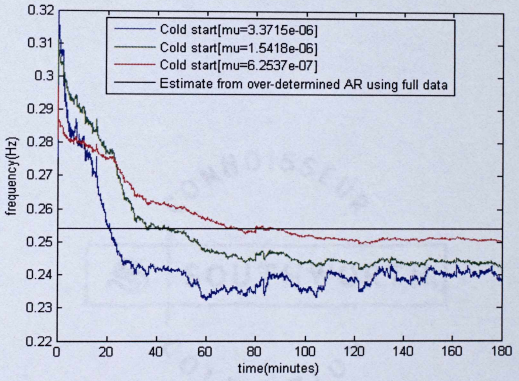

Figure 6.15: Mode frequency vs. time for MR #1 June 13, 2005 data (180 minutes, cold start: μ = 3.3715 e-06, 1.5418 e-06 and 6.2537 e-07).

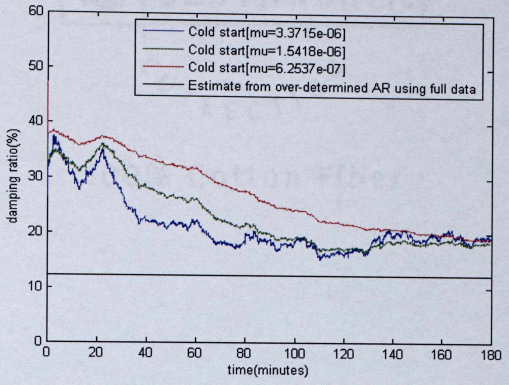

Figure 6.16: Mode damping ratio vs. time for MR #1 June 13, 2005 data (180 minutes) (cold start: μ = 3.3715 e-06, 1.5418 e-06 and 6.2537 e-07).

Figure 6.15 shows that as the step size parameter decreases the variability of the LMS estimate decreases, but the time taken by the estimate in converging increases. This is because of the inverse relationship between the time constant of the LMS filter and the step size parameter.

6.2.3 LMS Results with Previous Estimates from AR Block-processing

Figures 6.15 and 6.16 show that the LMS estimates of mode frequency and damping ratio with a cold start are variable and the time taken by them to converge to the AR estimates is longer than the data length. Using initial weight vector estimates from AR block-processing is one possible solution for getting the LMS estimates to converge faster with less variability. Figures 6.17 and 6.18 show the comparison of mode frequency and damping ratio estimates, respectively, with estimates from AR block-processing for different block sizes (10, 30, 90, 150 and 180 minutes). The step size

parameter was reduced by a factor of 10 (1.5418 e-07) from the best estimate case using the cold start LMS.

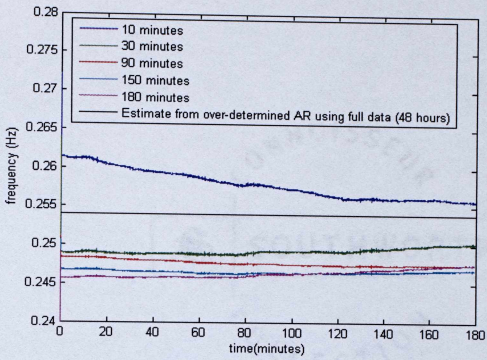

Figure 6.17: Mode frequency vs. time for MR #1 June 13, 2005 data (180 minutes, μ = 1.5418 e-07, weight vector from AR for different block sizes).

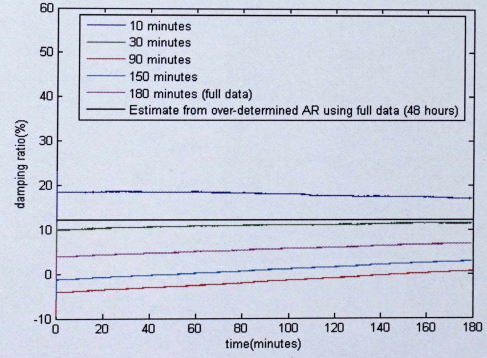

Figure 6.18: Mode damping ratio vs. time for MR #1 June 13, 2005 data (180 minutes, μ = 1.5418 e-07, weight vector from AR for different block sizes).

The information gained from Figures 6.17 and 6.18 is that both mode frequency and damping ratio LMS estimates using a weight vector from the AR estimate with a 30 minute block size is close to the AR estimates using the full 48 hours of data. Figure 6.18 shows that as the block size used for the AR block-processing increases the LMS estimates using initial AR estimates move closer to the estimate from the over-determined AR using the full block size. The LMS algorithm was reapplied to the same data block with initial weight vector estimates from 10 minutes into the previous LMS run. The step size parameter was reduced by a factor of 10 compared to the cold start LMS case (1.5418 e-07). Figures 6.19 and 6.20 show a comparison of LMS estimates for mode frequency and damping ratio, respectively, using a cold start, using an initial weight vector from 10 minutes into the previous run and using an initial weight vector from AR block-processing with a 10 minute block size.

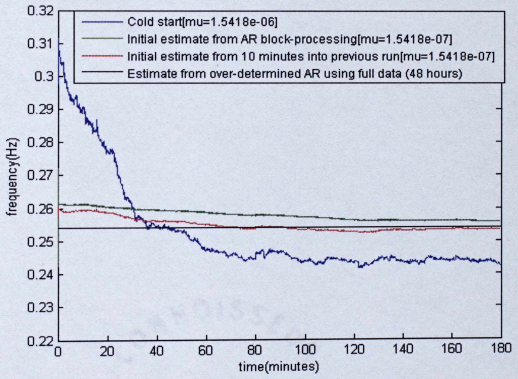

Figure 6.19: Mode frequency vs. time for the MR #1 June 13, 2005 data, using cold start, using an initial weight vector from 10 minutes into the previous run, and using an initial weight vector from AR block-processing with a 10 minute block size.

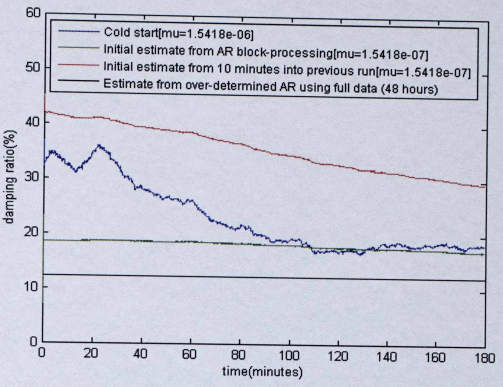

Figure 6.20: Mode damping ratio vs. time for the MR #1 June 13, 2005 ambient data using cold start, using an initial weight vector from 10 minutes into the previous run, and using an initial weight vector from AR block-processing with a 10 minute block size.

In the frequency estimates from Figure 6.19, not much difference is observed between the LMS estimates using the initial weight vector from AR block-processing and the LMS estimate using the initial weight vector from the previous LMS run. Figure 6.20 shows that the best results are obtained by using the initial weight vector estimates from AR block-processing. Using the initial weight vector from the previous LMS run heavily depends upon the step size parameter used in both the previous and the current LMS run. In cases of poor selection of previous LMS step size as in Figure 6.20, LMS estimates deteriorate in terms of convergence time.

However, the use of initial weight vector estimates from AR block-processing helps the LMS algorithm to converge with less variability. Since the LMS estimates are compared to the estimates from AR block-processing using a full block of data, then using an initial weight vector estimate for the LMS that is approaching the estimate for the full block AR estimate, the LMS estimate will approach that same value.

6.2.4 Results from ASLMS Algorithm

The 0.2540 Hz mode with a damping ratio of 12.12 % was set to be tracked by the ASLMS algorithm. As discussed in the introduction of Chapter 6 and as shown in Table 6.1 the degree of non-stationarity of the June 13, 2005 MR #1 data is 0.8867. Thus, the minimum misadjustment that can be achieved by the ASLMS algorithm is 0.7862. The smaller the value of misadjustment parameter compared to unity, the better the performance of an adaptive algorithm will be. The minimum misadjustment that can be achieved by the adaptive filter in working with the MR #1 June 13, 2005 data is closer to unity as opposed to the lower value of misadjustment for the MR #1 June 7, 2000 data.

Figures 6.21 and 6.22 represent the estimates of frequency and damping ratios, respectively, using the LMS and the ASLMS algorithms with a cold start. The value of the step size parameter μ used in these algorithms was set to 3.3715 e-06. The small positive constant ρ for the frequency estimate was set to 5.43 e-10 in Figure 6.21 and 6.94 e-10 for the damping ratio estimate in Figure 6.22. In terms of convergence time of the estimates, the ASLMS algorithm is expected to perform better than the LMS algorithm. However, due to the higher degree of non-stationarity and hence high misadjustment of the ASLMS algorithm, the ASLMS estimates of frequency and damping ratio do not show a considerable improvement in tracking performance compared to the cold start LMS case.

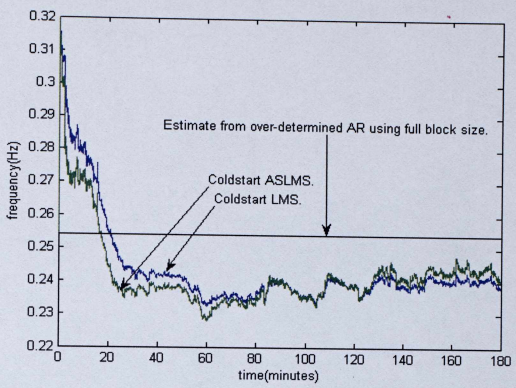

Figure 6.21: Mode frequency vs. time for MR #1 June 13, 2005 data (18.85 minutes, cold start, LMS: μ=3.3715 e-06, ASLMS: μ=3.3715 e-06, ρ= 5.43 e-10).

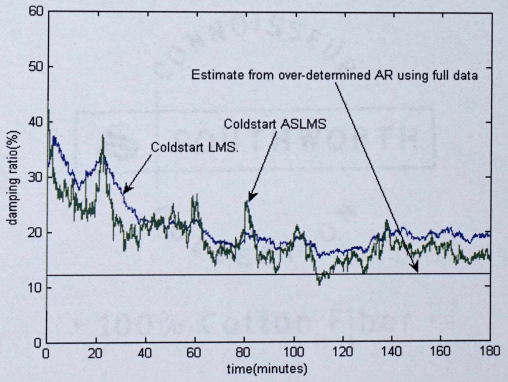

Figure 6.22: Damping ratio vs. time for MR #1 June 13, 2005 data (180 minutes, cold start, LMS: μ=3.3715 e-06, ASLMS: μ=3.3715 e-06, ρ= 6.94 e-10).

Figures 6.21 and 6.22 show that though the ASLMS algorithm helps the estimates approach closer to the AR estimate for the full block size faster than the LMS estimates, there is no considerable improvement seen in using the ASLMS algorithm as observed with the simulated and the MR #1 June 7, 2000 data set. This is due to the higher degree of non-stationarity of the MR #1 June 13, 2005 power system data. The more variability in the ASLMS estimates is due to the inherent error variance discussed in Chapter 4.

The small positive constant ρ is directly proportional to the step size parameter μ and it controls the adaptation of the ASLMS algorithm. Figures 6.23 and 6.24 show the frequency and damping ratio estimates, respectively, from ASLMS algorithm with a cold start using three different values of ρ. The three different values of ρ used for the frequency are 6.94 e-10, 5.43 e-10 and 2.50 e-10. The three values of ρ used for the damping ratio estimates shown in Figure 6.24 are 6.94 e-10, 5.31 e-10 and 2.38 e-10.

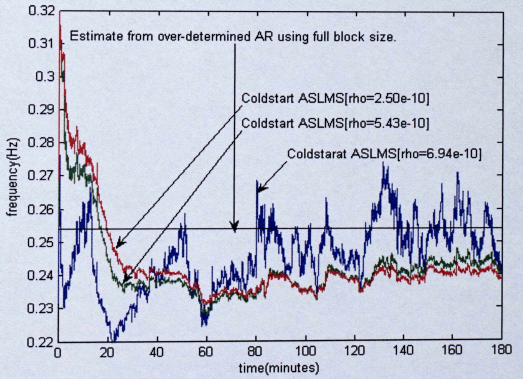

Figure 6.23: Mode frequency vs. time for MR #1 June 13, 2005 data (180 minutes, cold start, μ=3.3715 e-06 and ρ=6.94 e-10, 5.43 e-10 and 2.50 e-10).

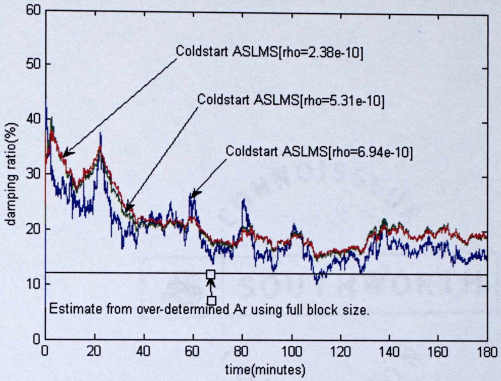

Figure 6.24: Damping ratio vs. time for MR #1 June 13, 2005 data (180 minutes, cold start, μ =3.3715 e-06 and ρ =6.94 e-10, 5.31 e-10 and 2.38 e-10).

The high degree of non-stationarity of the data used limited the range of the small positive constant that can be used with the ASLMS algorithm. Damping ratio estimates from the cold start ASLMS algorithm using ρ = 5.31 e-10 and 2.38 e-10 show no major difference in the estimates.

The three cases; 1) LMS-LMS, 2) LMS-ASLMS and 3) ASLMS-LMS explored with the MR #1 June 7, 2000 data were used with the MR #1 June 13, 2005 data. The step size parameter was reduced by a factor of 10 (3.3715 e-07) in all the three cases. Figures 6.25 and 6.26 show a comparison of mode frequency and damping ratio estimates, respectively, for the three above mentioned cases. The value of ρ used in the frequency estimate for case 2 is 1.53 e-07 and for case 3 is 2.5 e-08. The value of ρ used in the damping ratio estimate for case 2 is 1.12 e-07 and for case 3 is 4.08 e-08.

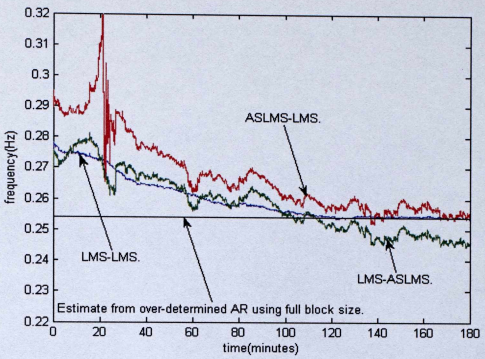

Figure 6.25: Mode frequency vs. time for MR #1 June 13, 2005 data (180 minutes, μ=3.3715 e-07, LMS-ASLMS: ρ=1.53 e-07 ASLMS-LMS: ρ=2.5 e-08).

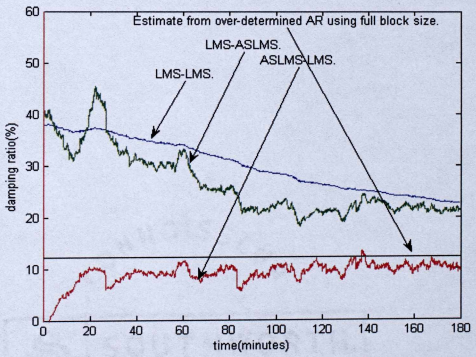

Figure 6.26: Damping ratio vs. time for MR #1 June 13, 2005 data (180 minutes, μ=3.3715 e-07, LMS-ASLMS: ρ=1.12 e-07, ASLMS-LMS: ρ=4.08 e-08).

The ASLMS-LMS case gives the best results in Figure 6.26 and converges in almost the same time as the LMS-LMS algorithm to the actual AR estimates using the full block size. The LMS-ASLMS estimates in Figure 6.25, however, move away from the actual estimate. Using the initial estimate of the weight vector from the ASLMS algorithm (case 3) produces an initial estimate near the AR estimate. However, due to the nature of the non-stationarity of the data in this case the ASLMS algorithm performs no better than LMS algorithm in terms of time of convergence of the estimates.

6.3 Performance of Error Tracking Algorithm

The error tracking algorithm combines the quicker convergence behavior of the ASLMS algorithm and less variable estimate of the LMS algorithm. Both the MR #1 June 7, 2000 and the MR #1 June 13, 2005 data were reapplied to the ET algorithm. Figure 6.27 and 6.28 show the frequency and the damping ratio estimates, respectively, of the ET algorithm. The value of step size μ used to start the ASLMS algorithm was 8.7448 e-07 in both the frequency and damping ratio estimates. The step size was further reduced by a factor of 10 while the ET algorithm continued tracking with the LMS algorithm. As the value of the estimation error decreases and the mode estimates fall between 99% and 101% of the actual value, the ET algorithm switches computation methods from the ASLMS to the LMS algorithm with a 10 times reduced step size for less variable results. The higher the value of the small positive constant used to start the ASLMS algorithm the quicker the ET estimates will fall within $\pm 1\%$ away from the actual value. Figures 6.29 and 6.30 show the frequency and damping ratio estimates, respectively, of the MR #1 2005 data using the ET algorithm.

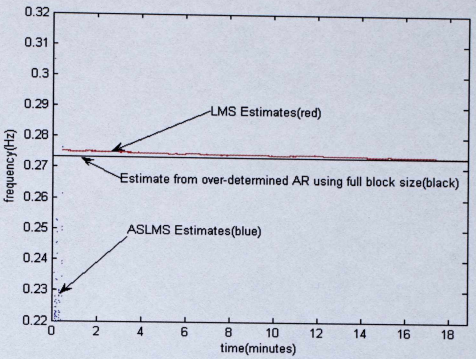

Figure 6.27: Mode frequency vs. time for MR #1 June 7, 2000 data (18.85 minutes, cold ASLMS start ASLMS: μ=8.7448 e-07, ρ=6.25 e-05 and LMS: μ=8.7448 e-08).

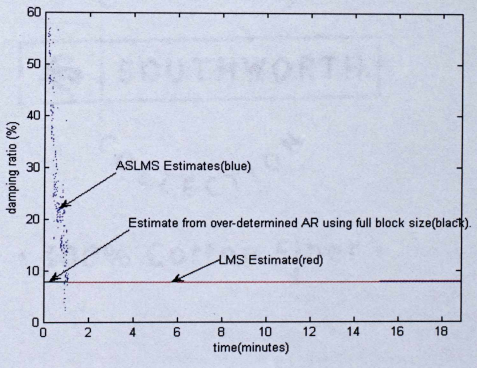

Figure 6.28: Damping ratio vs. time for MR #1 June 7, 2000 data (18.85 minutes, cold ASLMS start ASLMS: μ=8.7448 e-07, ρ=1.00 e-05 and LMS: μ=8.7448 e-08).

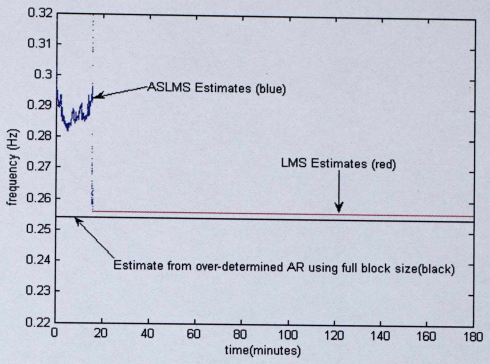

Figure 6.29: Mode frequency vs. time for MR #1 June 13, 2005 data (180 minutes, cold ASLMS start ASLMS: μ=3.3715 e-07, ρ=4.08 e-08 and LMS : μ=3.3715 e-08).

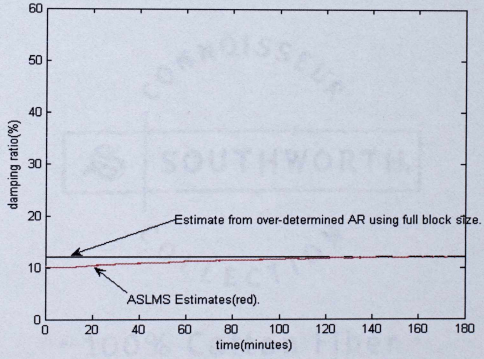

Figure 6.30: Damping ratio vs. time for MR #1 June 13, 2000 data (180 minutes, cold ASLMS start ASLMS: μ=3.3715 e-07, ρ=4.25 e-08 and LMS: μ=3.3715 e-08).

Chapter 7

Conclusions and Future Work

7.1 Conclusions

This work involved the use of adaptive filtering techniques based on Least Mean Squares (LMS) algorithms to estimate the electromechanical modes from both simulated and ambient power system data. The simulated system was a reduced order model of the western North American Power Grid. The real-time (ambient) data were taken from monitors in the western North American grid. Both the simulated and the ambient power system data had a dominant mode frequency at 0.26 Hz. Current methods of using these techniques have seen problems associated with the variability and the convergence time of the estimates. This work introduces a combination of LMS and Auto-Regressive (AR) block-processing techniques to overcome the constraints arising due to time of convergence and variability of the estimates. An Adaptive Step Size Least Mean Squares (ASLMS) algorithm was also introduced in this work to achieve high accuracy in mode estimation in the non-stationary environments.

The selection of the step size parameter was a crucial decision to be made when the LMS algorithm and the combination of algorithms were applied to both the simulated and ambient power system data. The performance of the LMS algorithm was measured on the basis of the variability of the estimates and the time of convergence. The frequency and damping ratio estimates from the LMS algorithm using zero initial weight vectors were less variable while weight vector estimates from the AR block-processing were used to start the LMS algorithm. Also the time of convergence of frequency and damping ratio estimates were reduced when initial estimates from the AR block-processing algorithm were used in the LMS algorithm. The selection of block size was a critical factor in using the AR block-processing algorithm. The standard deviation of the frequency and damping ratio LMS estimates from the actual value of mode frequency

and damping ratio, respectively, reduces as the block size used for initial AR block-processing estimates increases. This result agreed with the results presented in [20].

Use of an initial weight vector from the previous LMS run also helped the LMS estimates to achieve less variability and quicker convergence to the actual values of frequency and damping ratio. However, the frequency and damping ratio estimates from the LMS algorithm using initial estimates from AR block-processing with a 10 minute block size were closer to the actual value compared to the estimates of the LMS algorithm using initial estimates from 10 minutes into the previous LMS run. Also the selection of the step size parameter for the previous LMS algorithm played a crucial role in the accuracy of the LMS estimates using initial estimates from the previous LMS algorithm. The proper selection of step size will result in cases similar to Figure 6.19 in Section 6.2.3. The accuracy of the AR block-processing frequency and damping ratio estimates moved close to the actual value of frequency and damping ratio in the 19-machine test data case as the numerator co-efficient N and the correlation length K increased. However, the choice of N and K in the initial AR estimates did not have a considerable effect on the LMS estimates of frequency and damping ratio.

An Adaptive Step Size Least Mean Squares (ASLMS) algorithm is also used in this work to achieve high accuracy in the mode estimates. Along with the selection of step size parameter the selection of a small positive constant ρ also played an important role in the convergence behaviors of the ASLMS algorithm. Three different combinations of LMS and ASLMS algorithms were tested to achieve high accuracy in mode estimation (LMS-LMS, LMS-ASLMS and ASLMS-LMS). The case using initial estimates from the ASLMS algorithm in the LMS algorithm (ASLMS-LMS) achieved faster convergence (50% of time taken by other combinations) than LMS-ASLMS and LMS-LMS cases. The LMS-ASLMS case achieved better convergence performance than the LMS-LMS case in terms of convergence time. The estimates using the ASLMS algorithm were more variable than the ordinary LMS estimates for the same value of step size, because of the presence of irreducible error variance. Another important point to be noticed in using the ASLMS algorithm is the degree of non-stationarity of the environment. The ASLMS

algorithm designed to work in a non-stationary environment does not encourage good convergence behavior in environments where the degree of non-stationarity is high. The results in Section 6.2 are classical examples of this case. The use of initial estimates from AR, LMS and ASLMS algorithms in LMS algorithms improves the performance of the LMS tracking algorithm, but requires extra computation time in estimating the modes.

This work also introduced the Error Tracking (ET) algorithm, which is a combination of ASLMS and LMS algorithms that does not involve extra computation time like the other techniques mentioned above, if the exact value of frequency and damping ratio of the mode is known. The ET algorithm keeps track of the estimation error. Whenever the ASLMS algorithm estimates fall between 99% and 101% of the actual desired value, the ET algorithm switches computation from ASLMS to LMS algorithms. The ET algorithm combines the fast convergence performance of the ASLMS with the lower variability performance of the LMS algorithm.

In terms of time of convergence of the frequency and damping ratio estimates the cold start ASLMS algorithm converges faster than the cold start LMS algorithm. The ASLMS-LMS case further improves the convergence time and converges faster than the cold start ASLMS case. The ET algorithm takes the least time to converge compared to all the other algorithms.

In terms of variability of frequency and damping ratio estimates the cold start LMS algorithm performs better than the cold start ASLMS algorithm with less variability in its estimates. Using an initial weight vector from other algorithms (AR-LMS, ASLMS-LMS, and LMS-ASLMS) reduces the variability of both the LMS and ASLMS estimates compared to their corresponding cold start cases. The ET algorithm, however, tracks the frequency and damping ratio of the modes with the least variability compared to all the other cases mentioned above.

7.2 Future Work

As far as the LMS algorithm is concerned, further study is needed in the selection of an appropriate step-size parameter. The selection of the small positive constant ρ for the ASLMS is also an important factor to be further analyzed. The application of other adaptive methods like the normalized LMS (NLMS) and the recursive least squares (RLS) also can be explored for better convergence performance. The use of recursive methods like steepest descent could also be studied for mode estimation purposes as they track the time variations in the signal without having to solve the Wiener-Hopf equation and also the solution of the steepest descent algorithm terminates at the Wiener solution. Combinations of recursive algorithms and stochastic gradient algorithms like the steepest descent and the LMS algorithms, respectively, can also be explored.

The overall results from this work show that the use of adaptive algorithms and the use of a combination of algorithms allow tracking the electromechanical mode over time with improved convergence time and less variability in the estimates compared to the previous works. However, further work has to be done in tracking a mode that changes with time after a system disturbance and to track a moving mode.

Multi channel analysis of the modes should also be studied so that the frequency and damping ratio of a mode are not only analyzed from one point in the grid, but are analyzed from different points in the grid. If the time variation in the data does not disrupt the performance of these algorithms, they could be incorporated in Power Measurement Units (PMU's) like mode meters so that the electromechanical mode can be monitored over time and possible black-outs due to large oscillations can be prevented.

References

1. R. W. Wies, "Estimating Low-Frequency Electromechanical Modes of Power Systems Using Ambient Data," *Ph. D. Dissertation*, *Dept. Electrical Eng.*, University of Wyoming, Laramie, WY, 1999.
2. P. M. Anderson, "Power System Protection," IEEE Press, Piscataway, NJ, 1999, pp. 858-862 and 897-901.
3. V. Vittal, "Transient Stability and Control of Large Scale Power Systems," *Power Systems Engineering Research Center,* Iowa State University, Sep 4, 2003.
4. L. Kiss, "Inter-area Oscillations in Large Electric Power Systems," available at http://www.vmt.bme.hu/staff/kiss/topics/kl-inter.html, accessed on 02/05/06, *Dept. of Electric Power Systems*, Budapest University of Technology and Economics.
5. Y. J. Cao and Q. H. Wu , L. Jiang and S. J. Cheng, "Non linear control of power system multi-mode oscillations," *Electrical Power and Energy Systems*, Vol. 20, No. 1 , pp. 61- 68, 1998.
6. M. Klein, G. J. Rogers, and P. Kundur, "A Fundamental Study of Inter-Area Oscillations in Power Systems," *IEEE Transactions on Power Systems*, Vol. 6, No. 3, pp. 914-921, Aug. 1991.
7. J. F. Hauer and R. L. Cresap, "Measurement and Modeling of Pacific AC Intertie Response to Random Load Switching," *IEEE Transactions on Power Apparatus and Systems*, Vol. PAS-100, pp. 353-359, Jan. 1981.
8. J. W. Pierre, D. J. Trudnowski, and M.K. Donnelly, "Initial Results in Electromechanical Mode Identification from Ambient Data," *IEEE Transactions on Power Systems*, Vol. 12, No. 3, pp. 1245-1251, August 1997.
9. D. J. Trudnowski and J. E. Dagle, "Effects of Generator and Static-Load Nonlinearities on Electromechanical Oscillations," *IEEE Transactions on Power Systems*, Vol. 12, No. 3, pp. 1283-1288, Aug. 1997.

10. V. Vittal, N. Bhatia, and A. A. Fouad, "Analysis of the Inter-Area Mode Phenomenon in Power Systems Following Large Disturbances," *IEEE Transactions on Power Systems*, Vol. 6, No. 4, pp. 1515-1521, Nov. 1991.
11. K. R. Padiyar, *Power System Dynamics: Stability and Control*, New York: John Wiley & Sons, Inc., 1996.
12. G. R. B. Prony, "Essai Experimental et Analytique," J. l'Ecole Polytech, Paris, Vol. 1, pp. 24-76, 1795.
13. J. F. Hauer, C. J. Demeure, and L. L. Scharf, "Initial Results in Prony Analysis of Power System Response Signals," *IEEE Transactions on Power Systems*, vol. 5, Feb. 1990, pp. 80-89.
14. N. Zhou, J. W. Pierre, "Electromechanical Mode Estimation of Power Systems from Injected Probing Signals Using a Subspace Method," *Proceedings of the 2004 North American Power Symposium,* Moscow, Idaho.
15. J. R. Smith, C. S. Woods, F. Fatehi, G. L. Keenan, and J. F. Hauer, "A Low Order Power System Model with Dynamic Characteristics of the Western North American System," *Proceedings of the 1994 North American Power Symposium*, Manhattan, Kansas, Sept. 1994.
16. G. J. Rogers, *Power Systems Toolbox (PST)*, Cherry Tree Scientific Software, 1998.
17. S. Haykin, *Adaptive Filter Theory*, *Fourth Edition,* Pearson Education, 2002.
18. R. W. Wies, J. W. Pierre and D. J. Trudnowski "Use of LMS Adaptive Filtering Technique for Estimating Low-Frequency Electromechanical Modes of Power Systems," *Proceedings of the IEEE Power Meeting*, Denver, CO, June 2004.
19. P. O'Shea, "The Use of Sliding Spectral Windows for Parameter Estimation in Power System Disturbance Monitoring," *IEEE Transactions on Power Systems*, Vol. 15, No. 4, pp. 1261-1267, Nov. 2000.
20. R. W. Wies, J. W. Pierre, and D. J. Trudnowski, "Use of ARMA Block Processing for Estimating Stationary Low-Frequency Electromechanical Modes

of Power Systems," *IEEE Transactions on Power Systems*, Vol. 18, No. 1, pp. 167-173, Feb. 2003.

21. P. Stoica and R. Moses, *Introduction to Spectral Analysis*, Upper Saddle River, NJ: Prentice-Hall, 1997.
22. A. A. Beex and L. L. Scharf, "Covariance Sequence Approximation for Parametric Spectrum Modeling," *IEEE Transactions on Acoustics, Speech, and Signal Processing,* ASSP-29(5), pp. 1042-1052, 1981.
23. S. M. Kay, *Modern Spectral Estimation: Theory and Application*, Englewood Cliffs, NJ: Prentice Hall, 1988.
24. A. Papoulis and S. U. Pillai, *Probability, Random Variables and Stochastic Processes,* 4th ed., McGraw-Hill Edition, 1997.